CHARLES UNIVERSITY
Faculty of Science
Department of Parasitology

Study programme: Biology
Branch of study: Parasitology

Bc. Marie Zelená

Functional study of the SUF pathway in the cell of *Monocercomonoides exilis* and *Paratrimastix pyriformis*

Funkční analýza SUF dráhy v buňce *Monocercomonoides exilis* a *Paratrimastix pyriformis*

DIPLOMA THESIS

Supervisor: doc. Mgr. Vladimír Hampl, Ph.D.
Consultant: Carmen Priscila Peña-Diaz, Ph.D.

Praha 2020

Prohlášení:

Prohlašuji, že jsem závěrečnou práci zpracoval/a samostatně a že jsem uvedl/a všechny použité informační zdroje a literaturu. Tato práce ani její podstatná část nebyla předložena k získání jiného nebo stejného akademického titulu.

V Praze dne 8. 6. 2020 …….

Marie Zelená

Acknowledgements:

Firstly, I would like to thank my supervisor, doc. Mgr. Vladimír Hampl, Ph.D., for his time and scientific advice, as well as for allowing me to be a part of his team during my bachelor and master studies. The same amount of gratitude belongs to my consultant Priscila Peña Diaz, Ph.D., for sharing her practical skills and teaching me all the methods used in this thesis. Another thank you belongs to doc. RNDr. Ivan Hrdý, Ph.D., for providing his time and FPLC equipment for size-exclusion chromatography, and to Zuzana Vaitová, Ph.D. for providing *T. vaginalis* cultures and advising me how to work with them. Last but not least, I would like to thank all the brilliant people from the department of parasitology for creating a cheerful workplace and making my time in the department memorable.

Abstract

The synthesis of iron-sulfur clusters is an essential cellular process, which depends on complex biosynthetic pathways. In model eukaryotes, these pathways are the ISC pathway in the mitochondria and the CIA pathway in the cytosol. A recent genome and transcriptome analysis showed, that an amitochondriate protist *Monocercomonoides exilis* lacks the canonical ISC pathway, which has been replaced by a bacterial SUF pathway. A close free-living relative of *M. exilis*, *Paratrimastix pyriformis* possesses a mitochondrion-related organelle, yet also possesses a SUF pathway instead of ISC. The acquisition of the SUF pathway has been suggested as the primordial cause for mitochondrial loss in *M. exilis,* which is the first documented eukaryotic organism without a mitochondrion.

The SUF pathway has been the subject of numerous studies in bacteria, however, its role as the core provider of iron-sulfur clusters for eukaryotic cells has been reported in merely a handful of eukaryotes and was based predominantly on genomic data. This thesis focuses on the putative ATPase SufC and the putative scaffold protein SufB. Both proteins were successfully produced in recombinant forms. SufC has been found to possess ATPase activity *in vitro*, which was increased upon interaction with SufB. The conditions for the ATPase activity of SufC have been standardized. The recombinant form of SufC has been used to prepare an antibody, which was utilized to attempt the localization of the SUF pathway in the cell of both *M. exilis* and *P. pyriformis* with little success. An *in vitro* interaction between SufB and SufC from *M. exilis* has been proved using size exclusion chromatography, suggesting an *in vitro* formation of a complex with a size corresponding to either a $SufB_2C$ or $SufBC_2$ stoichiometry and its potential dimerization in the presence of ATP.

Abstrakt

Syntéza železo-sirných center je nepostradatelný buněčný proces, který je závislý na složitých biosyntetických drahách. U modelových eukaryot jsou těmito drahami ISC v mitochondrii a CIA v cytosolu. Nedávná analýza genomu a transkriptomu amitochondriálního prvoka *Monocercomonoides exilis* prokázala, že tento organismus postrádá ISC dráhu, která byla nahrazena bakteriální SUF dráhou. Blízký volně žijící příbuzný *M. exilis*, *Paratrimastix pyriformis*, obsahuje organely příbuzné mitochondrii, přesto zde byla ISC dráha také nahrazena dráhou SUF. Získání SUF dráhy je považováno za podmínku pro následnou ztrátu mitochondrie u *M. exilis*, který je prvním zdokumentovaným eukaryotickým organismem zcela bez této organely.

SUF dráha byla doposud předmětem mnoha studií u bakterií, avšak její role hlavního poskytovatele železo-sirných center pro eukaryotické buňky byla popsána pouze u několika případů, a to především na základě genomických dat. Tato práce se zabývá domnělou ATPázou SufC a domnělým proteinovým lešením SufB. Oba proteiny byly úspěšně izolovány v rekombinantní formě. U SufC byla naměřena ATPázová aktivita, která by zvýšená za přítomnosti SufB. Podmínky pro ATPázovou aktivity SufC byly standardizovány. Rekombinantní forma SufC byla použita k přípravě protilátky, která byla použita k lokalizaci SUF dráhy v buňkách *M. exilis* a *P. pyriformis*, bez zjevného úspěchu. *In vitro* interakce mezi SufB a SufC z *M. exilis* byla prokázána za použití gelové filtrace. Chromatografická data poukazují na *in vitro* tvorbu komplexu o velikosti odpovídající $SufB_2C$ nebo $SufBC_2$ stechiometrii a dimerizaci komplexu za přítomnosti ATP.

List of Abbreviations

ABC	ATP-binding cassette
ADP	adenosine diphosphate
ATCC	American-type culture collection
ATP	adenosine triphosphate
BSA	bovine serum albumin
cDNA	complementary DNA
CIA	cytosolic iron-sulfur cluster assembly
DAPI	4′,6-diamidino-2-phenylindole
DIC	differential interference contrast
DNA	deoxyribonucleic acid
EGTA	ethylene glycol tetraacetic acid, also known as egtazic acid
Fe-S	iron-sulfur (cluster)
FPLC	fast protein liquid chromatography
G418	Geneticin
HA-tag	hemagglutinin tag
HEPES	hydroxyethyl piperazine ethanesulfonic acid
His-tag	polyhistidine tag
HRP	horseradish peroxidase
IPTG	isopropyl ß-D-1-thiogalactopyranoside
ISC	iron-sulfur cluster
LB	lysogeny broth
LGT	lateral gene transfer
L-LDH	L-lactate dehydrogenase
MCS	multiple cloning site
MDG	minimal medium
MRO	mitochondrion-related organelle
MW	molecular weight

MWCO	molecular weight cut-off
NAD	nicotinamide adenine dinucleotide
NADH	nicotinamide adenine dinucleotide, reduced
NIF	nitrogen fixation
Ni-NTA	nickel nitrilotriacetic acid
OD	optical density
PBS	phosphate-buffered saline
PCR	polymerase chain reaction
PEM	PIPES, EGTA, $MgSO_4$ buffer
PEMBALG	PEM, BSA, lysine, gelatine buffer
PEP	phosphoenolpyruvate
PIPES	piperazine-N, N′-bis 2-ethane sulfonic acid
PK	pyruvate kinase
PLP	pyridoxal 5′-phosphate
PVDF	polyvinylidene difluoride
RNA	ribonucleic acid
RT	room temperature
SDS-PAGE	sodium dodecyl sulfate-polyacrylamide gel electrophoresis
SEC	size exclusion chromatography
SOC	super optimal broth with catabolite repression
SUF	sulfur utilization factors
SYBR	Synergy Brands
TAE	Tris base, acetic acid and EDTA buffer
TCA cycle	tricarboxylic acid cycle (citrate cycle)
Tris	tris(hydroxymethyl)aminomethane
tRNA	transfer RNA
TWEEN 20	polysorbate 20

TYM	trypticase-yeast-mucin medium
TYSGM	trypticase-yeast extract-serum-gastric mucin medium
UV-Vis	ultraviolet-visible spectroscopy
βME	β-mercaptoethanol

Contents

1 Introduction

Monocercomonoides exilis is a microaerophilic flagellate protist, which inhabits the large intestine of rodents, such as the long-tailed chinchilla (*Chinchilla lanigera*) (Nie 1950). This organism was recently found to be the first known eukaryote which possesses no mitochondria nor mitochondrion-related organelle (MRO) (Karnkowska et al. 2016). Since a microaerophilic or anaerobic lifestyle is believed to have led to the reduction of mitochondria to mitochondrion-related organelles in protists (ranging from anaerobic mitochondria to hydrogen-producing mitochondria, hydrogenosomes and mitosomes (Roger, Muñoz-Gómez, and Kamikawa 2017)), it is believed the ancestors of *M. exilis* possessed mitochondria, hence its loss is a secondary event. This theory is supported by the fact that a close free-living relative of *M. exilis*, *Paratrimastix pyriformis,* an inhabitant of freshwater anaerobic sediments, possesses a hydrogenosome-like MRO (O'Kelly, Farmer, and Nerad 1999).

The only known conserved function throughout almost all mitochondria and MROs is the synthesis of small inorganic cofactors called iron-sulfur clusters (Tachezy and Šmíd 2007). These cofactors are parts of many important proteins and play different roles such as electron transfer and iron homeostasis regulations. Pathways for the iron-sulfur cluster synthesis are present in all cells without exceptions. In model eukaryotic cells, iron-sulfur cluster synthesis is carried out in the mitochondrion via the ISC pathway, and in the cytosol via the CIA pathway, which is ISC pathway-dependent. The ISC pathway is present in virtually all mitochondria including the most reduced mitosomes. Both *M. exilis* and *P. pyriformis* lack the ISC pathway and instead possess a bacterial SUF pathway acquired via lateral gene transfer. Experiments with heterologous expression of *M. exilis* SUF pathway proteins in yeast and *T. vaginalis* suggest this pathway is localized in the cytosol. It is believed the acquisition of the SUF pathway by a common ancestor of *M. exilis* and *P. pyriformis* and its localization in the cytosol made the ISC pathway and the MRO of *M. exilis* ancestor dispensable, and ultimately led to the complete loss of mitochondria in this organism (Karnkowska et al. 2016). So far, these findings have been supported predominantly by genomic data, and no experiments have been conducted regarding the function of the SUF pathway in both *M. exilis* and *P. pyriformis*. As the main objective of this thesis I would like to provide experimental evidence for the function of the SUF pathway in *M. exilis* by characterizing the ATPase component SufC and its interaction with the scaffold protein SufB *in vitro*, as well as attempt to localize this pathway *in situ* in both *M. exilis* and *P. pyriformis.*

2 Review of literature

2.1 *Monocercomonoides exilis*

The genus *Monocercomonoides* belongs to the family Polymastigidae (Oxymonadida, Preaxostyla, Metamonada, Excavata). Oxymonads are a diverse group of flagellate protists which may be found in the digestive tract of both vertebrates and invertebrates. The largest diversity of oxymonads is in the hindgut of termites and wood-eating cockroaches, where these protists help their host in wood particle digestion and possibly the digestion of cellulose. Oxymonads are associated with diverse species of prokaryotic symbionts on their surface and inside their cells, which offers an interesting area for protistologists to research, but can make it difficult to establish these organisms in axenic culture (Hampl 2017; Treitli et al. 2019).

Monocercomonoides exilis (**Figure 1**) is a symbiont of the large intestine of caviomorph rodents such as guinea pigs and chinchillas (Nie 1950). The exact relationship between this protist and its host has not yet been described, however, it is believed to be commensalism rather than parasitism. The cell of *M. exilis* is relatively small (~6 μm) with four flagella and a complex cytoskeleton (Treitli et al. 2018). The most distinctive feature of this protist has been revealed in 2016 in its genome and transcriptome analysis, in which *M. exilis* was proven to be the very first known eukaryotic organism to completely lack a mitochondrion (Karnkowska et al. 2016). In these analyses, no mitochondria hallmark genes were found, including any parts of the Iron-Sulfur Cluster synthesis pathway (ISC). Iron-sulfur cluster synthesis is an essential part of all mitochondria and mitochondrion-related organelles, and at the same time, it is vital for all cells. Instead of the ISC pathway, components of the SUF (Sulfur Mobilisation) pathway were retrieved from *M. exilis* genome. Presumably, the SUF pathway was acquired by lateral gene transfer from bacteria and started producing iron-sulfur clusters in the cytosol, which lead to the ISC pathway no longer being essential for the cell. This could have led to the loss of ISC and the subsequent loss of mitochondria.

2.2 *Paratrimastix pyriformis*

Paratrimastix pyriformis (**Figure 1)** is a free-living flagellate protist, which inhabits anoxic sediments in freshwater environments. It belongs to the family Paratrimastigidae (Preaxostyla, Metamonada, Excavata) and it is a close free-living relative of oxymonads including *M. exilis* (Hampl 2017). Unlike *M. exilis*, this protist possesses mitochondria, more accurately mitochondrion-related organelles (MRO), which are morphologically similar to hydrogenosomes (O'Kelly, Farmer, and Nerad 1999). Similarly to *M. exilis*, no

signs of the ISC pathway were found in its genome, and this pathway was replaced by the SUF system. It is assumed that the SUF system was acquired by a common ancestor of these two organisms, leading to the loss of ISC in both, and the loss of mitochondria altogether in the case of *M. exilis* (Karnkowska et al. 2016; Vacek et al. 2018).

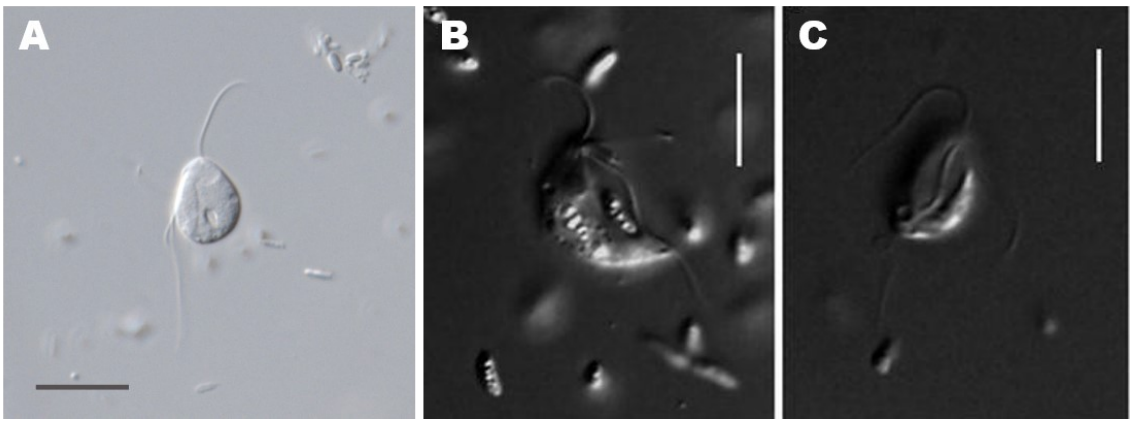

Figure 1: DIC images of *M. exilis* (**A**, adopted from Karnkowska and Hampl, 2017) and *P. pyriformis* (**B,** adopted from Hampl 2017). Size bars: 10 µm.

2.3 Iron-sulfur clusters

2.3.1 The function and structure of iron-sulfur clusters

Iron-sulfur clusters (Fe-S) are small inorganic cofactors composed of iron and inorganic sulfur. These prosthetic groups are vital parts of all cellular life forms on Earth. Many proteins that take part in essential cellular processes have an iron-sulfur cluster cofactor. In these proteins, iron-sulfur clusters perform diverse functions. Their best-known function is the transfer of electrons in the protein complexes of respiratory and photosynthetic electron-transport chains and redox enzymes (Broderick, 2003). However, iron-sulfur clusters may also act as enzyme catalytic centres, they can activate or inactivate enzymes by conversion to different oxidative states or ligand-exchange and can be inserted or removed from proteins (Beinert 1997). Some of these functions are utilized by proteins during essential processes such as DNA mismatch repair, citrate cycle, gene expression, regulation, tRNA modification and iron and oxygen sensing (Xu and Møller 2011). There are various types of iron-sulfur clusters. The most common are the rhombic [2Fe-2S] and cubane [4Fe-4S] clusters (**Figures 2** and **3**). More complex clusters are usually formed by the fusion of these simple clusters and can sometimes include other metals in their structure (Beinert 1997).

Figure 2: Rhombic [2Fe-2S] iron-sulfur cluster (adapted from Xu and Møller 2011).

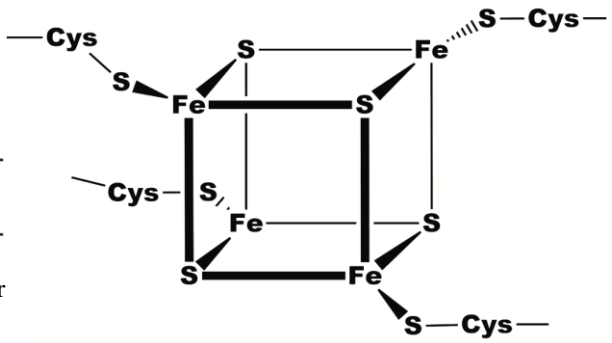

Figure 3: Cubane [4Fe-4S] iron-sulfur cluster (adapted from Xu and Møller 2011).

2.3.2 Iron-sulfur cluster synthetic pathways

The synthesis of iron-sulfur clusters is carried out by intricate biochemical machineries, all of which follow a general scheme outlined in **Figure 4** (Roche et al. 2013). A cysteine desulfurase cleaves sulfur from L-cysteine with a free L-alanine by-product. Iron is provided by a yet unconfirmed donor, however, iron-containing protein frataxin has been proposed to be the most probable source in the case of ISC (Stemmler et al. 2010). The cluster itself is then synthesized on a protein scaffold and subsequently, carrier proteins mediate the insertion of the cluster into target apoproteins (Roche et al. 2013).

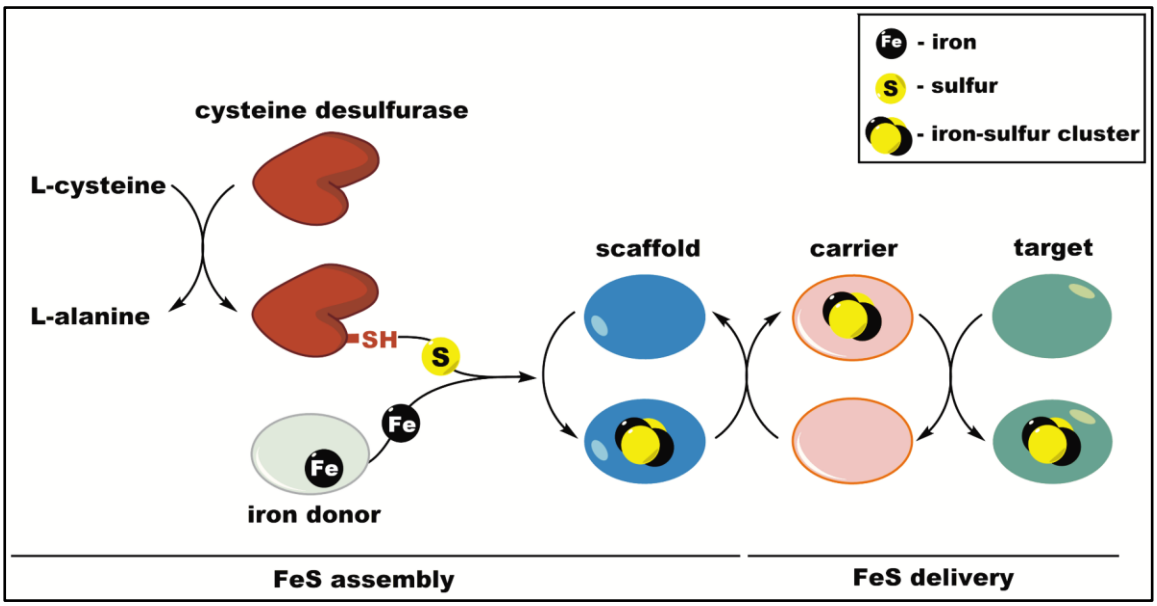

Figure 4: Schematic representation of iron-sulfur cluster synthesis. A cysteine desulfurase cleaves sulfur from L-cysteine whilst producing L-alanine. Iron is provided by a yet unknown donor. Iron-sulfur cluster is synthesized on a protein scaffold and carrier proteins facilitate insertion of the cluster into target apoproteins (adapted from Roche et al. 2013).

In prokaryotes, three different synthetic pathways are known. The iron-sulfur cluster pathway (ISC) is the so-called housekeeping system and forms most iron-sulfur clusters in bacteria. In *E. coli*, the SUF pathway is called upon to respond to iron starvation or oxidative stress (Blanc et al. 2014). Nitrogen fixation system (NIF) was described in nitrogen-fixing bacteria *Azotobacter vinelandii* for the assembly of nitrogenase (Jacobson et al. 1989). In model eukaryotic cells, such as the yeast *Saccharomyces cerevisiae,* iron-sulfur cluster synthesis is carried out by the ISC pathway in mitochondria. Cytosolic and nuclear iron-sulfur clusters are synthesized by the cytosolic iron-sulfur assembly pathway (CIA), which does not possess its own cysteine desulfurase and is solely dependent on a sulfur-containing compound provided by the ISC pathway.

2.3.3 The ISC pathway

The ISC pathway has been well described in both prokaryotic and eukaryotic model organisms. The eukaryotic mitochondrial ISC has been inherited from a prokaryotic ancestor of mitochondria (Sagan 1967). For a better understanding of evolutionary processes regarding the pathway, overviews of both prokaryotic ISC (as described in *Escherichia coli)* and eukaryotic ISC (as described in *Saccharomyces cerevisiae)* are provided in the following paragraphs.

2.3.3.1 The ISC pathway in E. coli

In the first step, sulfur is cleaved from L-cysteine by the IscS cysteine desulfurase. IscS is a pyridoxal-5'-phosphate (PLP)-depending enzyme and it cleaves sulfur from L-cysteine in the form of a persulfide. A by-product of this reaction is free L-alanine (Schwartz et al. 2000). Persulfide is then transferred from IscS to the scaffold protein, IscU, on which the [2Fe-2S] cluster assembly takes place (Urbina et al. 2001). A bacterial homolog of frataxin, CyaY, is involved in the cluster assembly as well. This is an iron-binding protein, which interacts with IscS *in vitro* and is believed to be the provider of iron for the cluster assembly (Adinolfi et al. 2009). [4Fe-4S] clusters are also produced on the IscU scaffold. This is achieved by the fusion of two [2Fe-2S] clusters, which is accompanied by their ferredoxin-mediated reduction (Chandramouli et al. 2007). The cluster is then released from the scaffold by a DnaK-type chaperone HscA, which is controlled by its DnaJ-type co-chaperone HscB, in an ATP-dependent process (Hoff, Cupp-Vickery, and Vickery 2003; Silberg et al. 2004). In the final step, the cluster is transferred to the apoprotein by two A-type carrier proteins. Firstly, the cluster is transferred from IscU to IscA, which further transfers the cluster to ErpA, facilitating the

insertion of the cluster into the recipient apoprotein (Loiseau et al. 2007; Gupta et al. 2009). An overview of the pathway is provided in **Figure 5**.

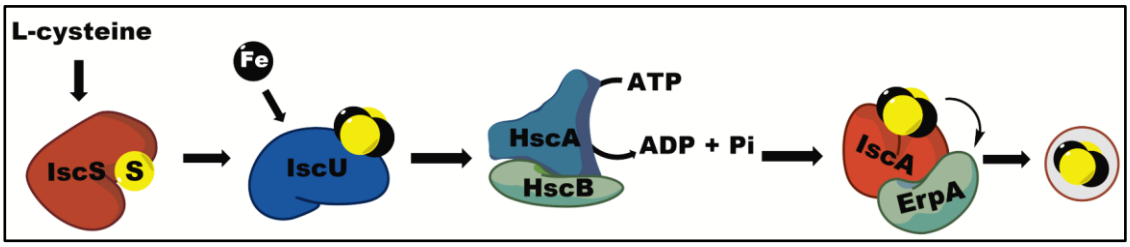

Figure 5: General scheme of the ISC pathway in *E. coli*. IscS cleaves sulfur from L-cysteine, the cluster is assembled by IscU. Chaperones HscA and HscB facilitate the release of the cluster from IscU and its transfer to carrier proteins IscA and ErpA, which transfer the cluster into recipient apoproteins (adapted from Roche et al. 2013).

2.3.3.2 The ISC pathway in S. cerevisiae

The eukaryotic version of the ISC pathway is slightly more complex than its ancestral prokaryotic counterpart (**Figure 6**). Most importantly, the mitochondrial ISC pathway is divided into two parts. The so-called "early ISC", mostly composed of proteins homologous to the prokaryotic ISC, is responsible for the formation of [2Fe-2S] clusters. The "late ISC machinery" follows the early one and assembles [4Fe-4S] clusters (Braymer and Lill 2017). The cysteine-desulfuration step in *S. cerevisiae* is carried out by an IscS-homologue called Nfs1, which acts as part of a larger complex accompanied by two proteins, Isd11 and the acyl carrier protein 1 (Acp1). These two proteins are unique to eukaryotes and do not have prokaryotic homologues. Although their precise function has not yet been described (Muhlenhoff 2003; Richards and van der Giezen 2006), Acp1 has been ascribed a regulatory role in cluster formation (Boniecki et al. 2017). The cluster formation step is executed by two IscU homologs, Isu1, and Isu2 (Muhlenhoff 2003). The source of iron for the assembly step remains uncertain, the most probable candidate seems to be frataxin (Yfh1, yeast frataxin homolog) (Stemmler et al. 2010). The assembly step is accompanied by a small electron-transport chain consisting of two proteins, ferredoxin (Yah1) and ferredoxin-reductase Arh1. This process is NADH-dependent. It has been speculated that this chain takes part in the reduction of sulfur (S^0 -> S^{2-}) however further studies would be required to support this theory (Lange et al. 2000; Sheftel et al. 2010; Shi et al. 2010). The release of the cluster from the scaffold is in this case also carried out by a DnaK-type chaperone, a HscA-homologue Ssq1. Ssq1 has two co-chaperones, a HscB-homologue Jac1 and a second co-chaperone MgeI. The process of cluster release is ATP-dependent, just like in *E. coli.* The ATPase activity of Ssq1 is accelerated by JacI.

MgeI replaces ADP of Ssq1 for ATP, thus regenerating its function (Uzarska et al. 2013). The [2Fe-2S] cluster is then received by Grx5 (monothiol glutaredoxin 5) which mediates the insertion of the cluster to recipient proteins throughout the mitochondria and provides the [2Fe-2S] to the late ISC (Brancaccio et al. 2014; Braymer and Lill 2017). The late ISC consists of a scaffold and many apoprotein-specific carriers. The scaffold is a complex, which consists of three A-type proteins, Isa1-Isa2-Iba57. Isa1 and Isa2 are homologs of bacterial IscA. The [4Fe-4S] clusters are formed by the coupling of two [2Fe-2S] clusters (Brancaccio et al. 2014; Braymer and Lill 2017). The insertion of the cluster into the apoprotein is carried out by many different carrier proteins such as Ind1 and Bol proteins (Braymer and Lill 2017).

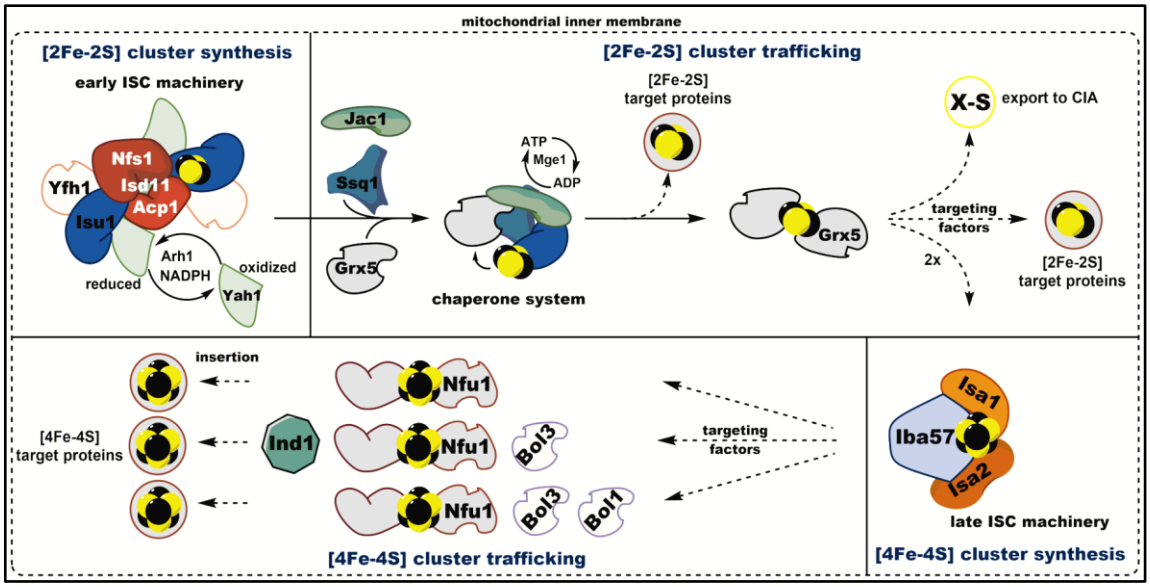

Figure 6: An overview of the ISC pathway from *S. cerevisiae.* [2Fe-2S] clusters are assembled by the early ISC machinery and [4Fe-4S] cluster are assembled by the late ISC machinery (adapted from Braymer and Lill 2017).

2.3.4 The CIA pathway

The CIA pathway (**Figure 7**) is a novelty of eukaryotes, which is used by the cell for iron-sulfur cluster assembly in the cytosol. The following description is corresponding to findings in *S. cerevisiae* and mice. The CIA pathway does not possess its own cysteine desulfurase, which is why it is dependent on the ISC to provide sulfur. The sulfur is provided by a yet undescribed sulfur-bearing molecule (often referred to as factor X, or X-S) which is synthesized by the ISC. The transfer of factor X from mitochondria is carried out by the ABC (ATP binding cassette) transporter Atm1 which is localized to the inner mitochondrial membrane (Pondarré et al. 2006; Kispal et al. 1999). The formation of the cluster takes place on the Cfd1-Nbp35 scaffold. The assembly is accompanied by

an electron transport chain consisting of Tah18 and Dre2. The resulting cluster is then inserted into the apoprotein by a carrier Nar1 and the CIA-targeting complex Cia1-Cia2-Mms19 (Lill et al. 2015).

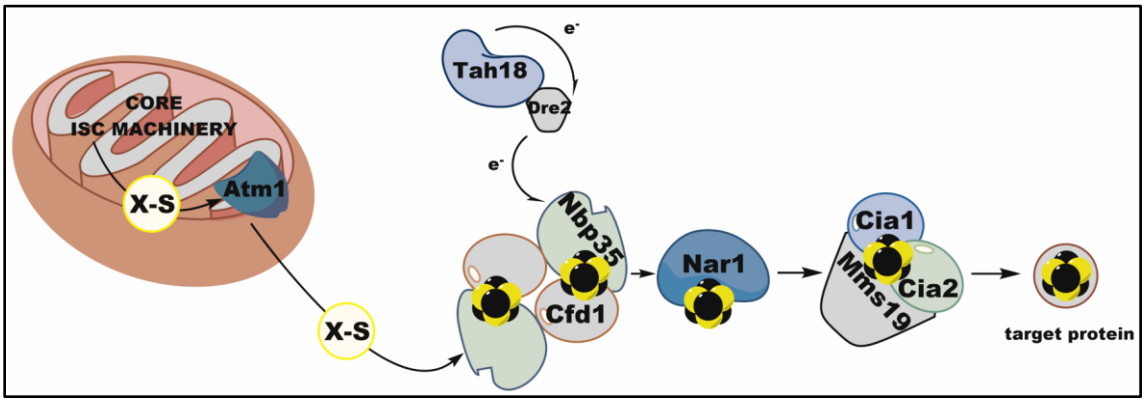

Figure 7: An overview of the CIA pathway. A sulfur-containing compound X-S is transferred from the mitochondrial ISC machinery to the cytosol by Atm1 carrier. X-S is utilised by Nbp35-Cfd1 complex for iron-sulfur cluster assembly. Nar1 carrier and CIA-targeting complex Cia1-Cia2-Mms19 facilitate the transfer of the cluster to recipient apoproteins.

2.3.5 The SUF pathway

The SUF pathway was first discovered in *E. coli* (Patzer and Hantke 1999), where it serves along the housekeeping ISC pathway as a backup in the case of iron starvation or oxidative stress. In some *Firmicutes* such as *Bacillus subtilis,* it was found to be the sole provider of iron-sulfur clusters (Reuß et al. 2016). This pathway is also found in many eukaryotes, most commonly in plastids of plants and algae, but also in the apicoplast of apicomplexan parasites (Ali and Nozaki 2013). Parts of this pathway were found in some eukaryotes without plastids, such as *Blastocystis, Stygiella,* and *Pygsuia,* and in those cases, the pathway is believed to be acquired via lateral gene transfer (Denoeud et al. 2011.; Tsaousis et al. 2012; Leger et al. 2016; Stairs et al. 2014). In *M. exilis* and *P. pyriformis* a more complete version of the pathway was found and together with CIA, it seems to be the sole provider of iron-sulfur clusters for the cell (Vacek et al. 2018).

The SUF pathway consists of two complexes (**Figure 8**). In *E. coli* the cysteine desulfurase SufS works in a heterodimer with its enhancer SufE (Outten et al. 2003). In some organisms such as *B. subtilis, M. exilis,* and *P. pyriformis*, SufE is substituted by SufU (Albrecht et al. 2010; Karnkowska et al. 2016). The cluster is assembled on the scaffold protein SufB, which is in a complex with two other proteins, SufC and SufD

(Wollers et al. 2010). SufA is a carrier protein, which cooperates with ErpA in *E. coli* (Gupta et al. 2009). All SUF pathway proteins are further described in detail below.

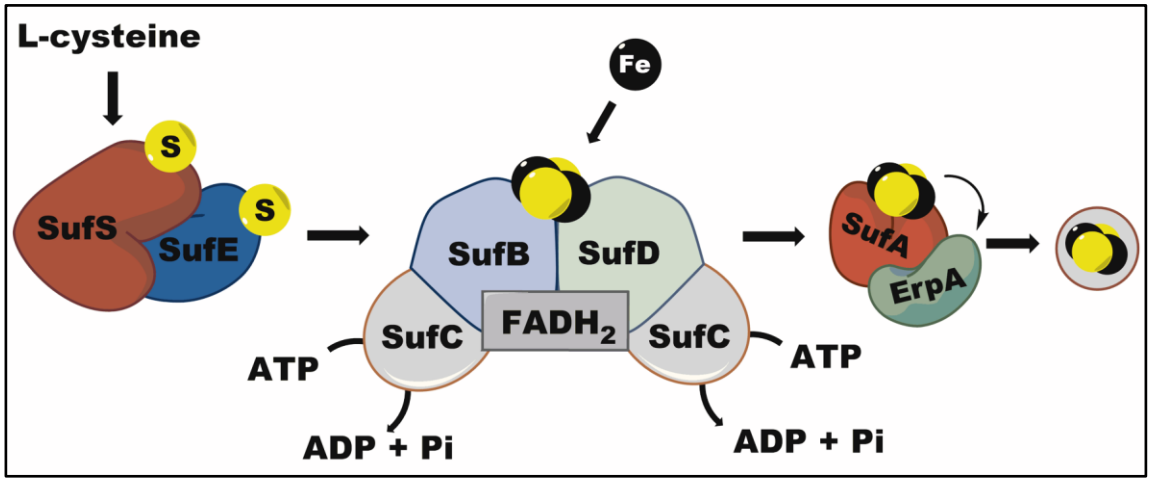

Figure 8: An overview of the SUF pathway from *E. coli*. Sulfur is cleaved from L-cysteine by a cysteine desulfurase SufS, which is in complex with its enhancer SufE. The cluster is assembled by a scaffold protein SufB and its interactors SufD and SufC. SufA interacts with ErpA and facilitates the transfer of the cluster to recipient apoproteins (adapted from Roche et al. 2013).

2.3.5.1 The cysteine desulfurase complex

2.3.5.1.1 SufS

SufS is the cysteine desulfurase of the SUF system (Kaiser et al. 2000). As a cysteine desulfurase, this enzyme is dependent on a PLP cofactor and cleaves sulfur from an L-cysteine molecule in the form of a transient persulfide with an L-alanine by-product. The cysteine-sulfur bond is broken by a conserved active site cysteine (Cys364 in *E. coli* SufS) (Cupp-Vickery, Urbina, and Vickery 2003). SufS is classified as a class II cysteine desulfurase, and as such, it contains a short, structurally defined Cys-loop. This short loop makes persulfide formation possible without a large conformational change, as it means that when L-cysteine binds to the PLP cofactor, the substrate thiol, and the catalytic Cys-thiol are in close enough proximity to allow persulfide bond formation (Black and Dos Santos 2015). The SufS cysteine desulfurase activity is greatly enhanced upon interaction with a sulfur acceptor, SufE, or SufU (Outten et al. 2003; Loiseau et al. 2003). A crystal structure of SufS from *E. coli* is described in **Figure 9** (Dunkle et al. 2019).

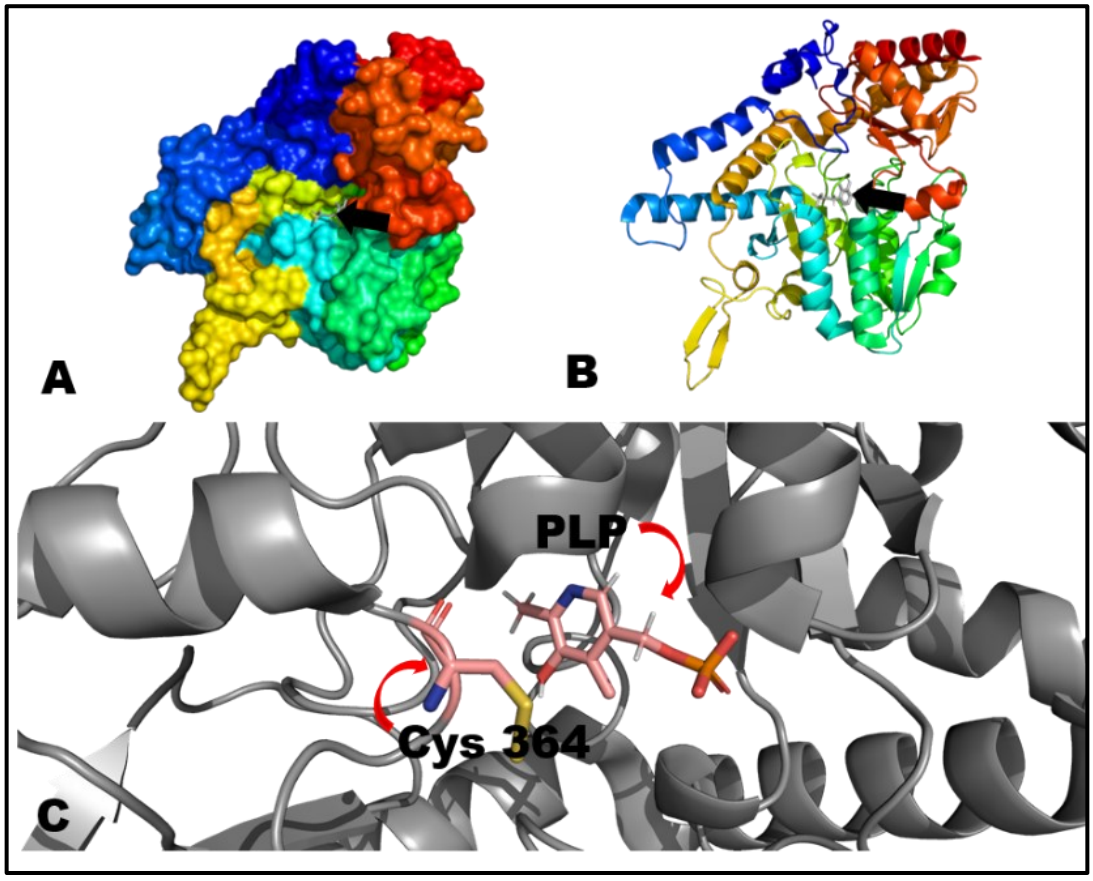

Figure 9: Crystal structure of SufS from *E. coli* (PDB ID: 6MR6, Dunkle et al. 2019). **A** – surface model; **B** – ribbon model, black arrows marks the active site; **C** – detail of the active site with pyridoxal-5´-phosphate (PLP) and conserved active-site cysteine with a persulfide bond (Cys364).

2.3.5.1.2 SufE

SufE is a sulfur acceptor protein, which interacts with SufS. SufE binds the persulfide molecule to its active cysteine site (Cys51 in *E. coli* SufE, **Figure 10**) (Loiseau et al. 2003) and transfers it to the scaffold complex (Layer et al. 2007).

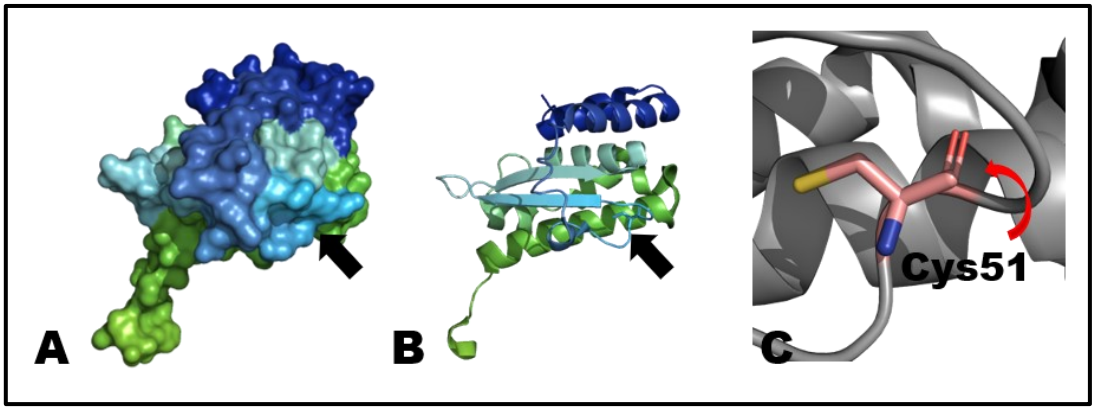

Figure 10: Crystal structure of SufE from *E. coli* (PDB ID: 1MZG, Goldsmith-Fischman et al. 2004). **A** – surface model; **B** – ribbon model, active site marked by black arrow; **C** – detail of the active site with active site cysteine (Cys51).

2.3.5.1.3 SufU

SufU is an alternative to SufE found in some organisms such as *B. subtilis* and *M. exilis.* Similarly to SufE, SufU binds to SufS and binds the persulfide to its active cysteine site (Cys41 in *B. subtilis,* **Figure 11)** (Fujishiro et al. 2017). SufE and SufU are non-homologous, however, their tertiary structure is very similar (Albrecht et al. 2010). In addition to the persulfide-binding active cysteine site, SufU possesses additional active cysteine sites, which form a zinc-binding site with the sulfur binding cysteine residue (Selbach et al. 2014).

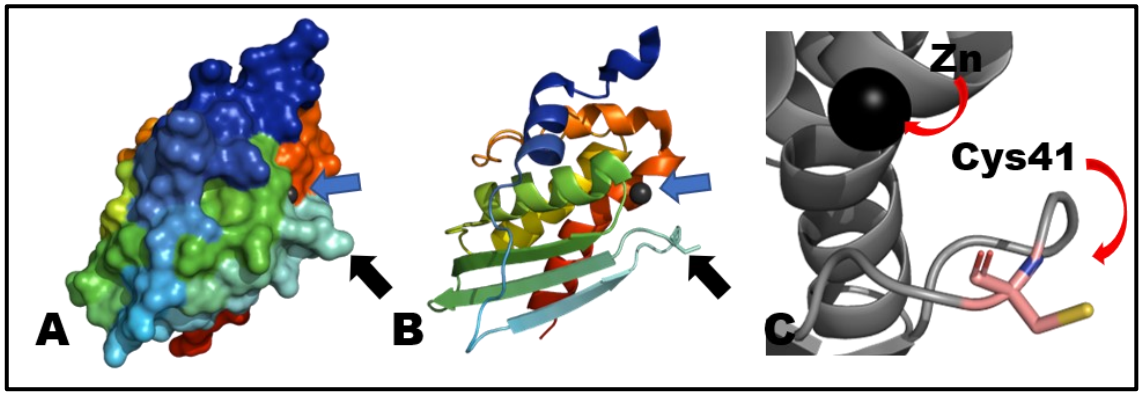

Figure 11: Crystal structure of SufU from *B. subtilis* (PDB ID: 5XT6, Fujishiro et al. 2017). **A** – surface model; **B** – ribbon model, active site marked by black arrow, zinc-binding site marked by blue arrow;, **C** – detail of the active site with active site cysteine (Cys41) next to the zinc-binding site with zinc (Zn).

2.3.5.2 Scaffold complex

2.3.5.2.1 SufB

SufB is the cluster-assembling member of the scaffold complex. It has not yet been determined what type of cluster SufB assembles *in vivo,* however, it was shown to form both a [2Fe-2S] and a [4Fe-4S] clusters *in vitro* (Hirabayashi et al. 2015). Both [2Fe-2S] SufB and [4Fe-4S] SufB forms were able to transfer their cluster to a target apoprotein (Watanabe, Kita, and Miki 2005). The only available crystal structure of SufB was obtained by isolation of the SufBCD complex (Figure 10) (Hirabayashi et al. 2015). The N-terminal part of SufB contains a canonical Fe-S binding motif (CxxCxxxC) (Layer et al. 2007). However, a recent study by Yuda et al., which mapped the key residues of SufB and SufD in *E. coli* found that this motif is dispensable for the protein's function. The residues proposed by this study to take part in the binding of the FeS cluster were Cys405, Glu434, His433, and Glu432. Two cysteine residues, Cys254 and Cys405, were proposed

to accept sulfur from SufE (Yuda et al. 2017). All mentioned residues are pointed out in **Figure 12** using the crystal structure of the SufBCD complex (Hirabayashi et al. 2015).

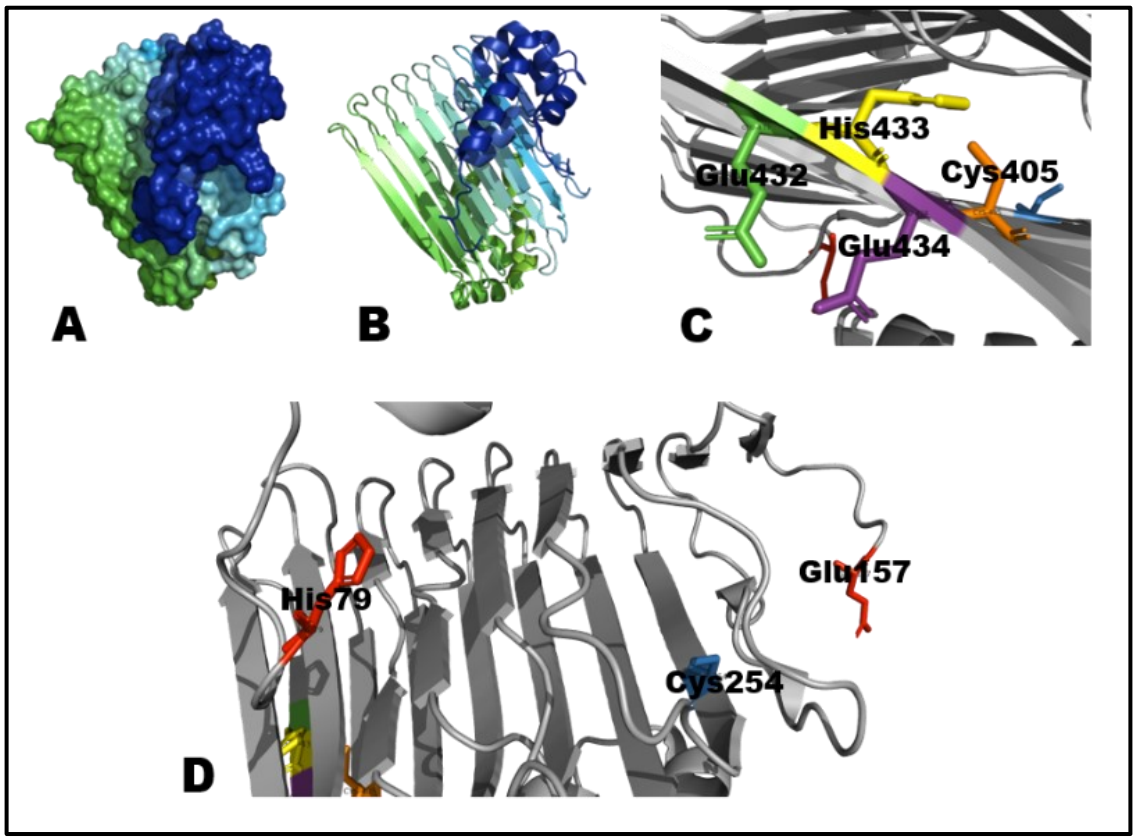

Figure 12: Crystal structure of SufB (PDB ID: 5AWF, Hirabayashi et al. 2015). **A** – surface model; **B** – ribbon model. **C** – functional residues proposed to take part in cluster binding (Cys405, Glu432, His433 and Glu434). Cys405 was also proposed to accept sulfur from SufE. **D** – Detail of N-terminal part of SufB. The region which contains the canonical FeS cluster binding motif (His79-Glu157) is disordered and invisible in the crystal structure. Cys254 is a residue proposed to take part in accepting sulfur from SufE.

2.3.5.2.2 SufC

SufC is an ATP-binding cassette (ABC) ATPase. As such it exhibits typical structures, such as Walker A and Walker B motifs and D- and Q-loops (Watanabe, Kita, and Miki 2005). SufC was found to possess ATPase activity (Nachin 2003) which is enhanced by the interaction with SufB and SufD (Petrovic et al. 2008; Tian, He, and Liu 2014). Tian, He and Liu demonstrated the doubling in *Thermus thermophilus* SufC ATPase activity upon interaction with SufB and SufD separately, which was further increased upon SufBCD complex formation. Petrovic et al. on the other hand documented that that the activity of SufC from *Thermotoga maritima* is increased 180-fold upon interaction with SufB and 5-fold upon interaction with SufD. Interestingly, the crystal structure of SufC showed an unusual conformation of a linker between ABC alpha and beta domains, which

seems to be well-suited for the interaction with these two proteins (**Figure 13**) (Watanabe, Kita, and Miki 2005).

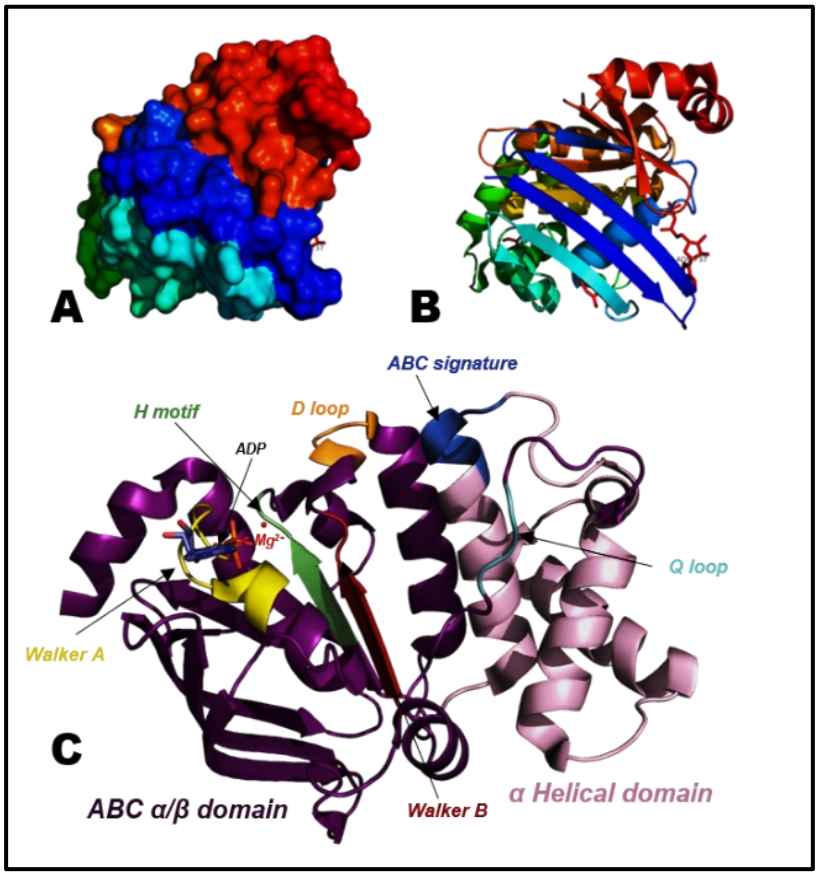

Figure 13: Crystal structure of SufC from *Thermus thermophillus* with a Mg^{+2} cofactor and ADP (PDB ID: 2D2F, Watanabe, Kita, and Miki 2005). **A** – surface model; **B** – ribbon model. **C** – ribbon model with labelled structures: The ABC α/β domain is shown in dark purple, the α helical domain in pink. The conserved ABC ATPase motifs are labelled as follows: **Walker A motif** (yellow); **Walker B motif** (red); **ABC signature motif** (blue); **Q loop** (lighter blue); **H motif** (green); and **D loop** (orange). The **ADP** molecule bound to SufC is represented in a stick model and **Mg^{2+}** cofactor is represented by a red ball. The motifs were labeled according to Watanabe, Kita and Miki 2005.

2.3.5.2.3 SufD

SufD is a paralogue of SufB, sharing 17% identity and 37% similarity in primary sequence (Garcia et al. 2019). The exact function of SufD has not yet been resolved, studies have suggested this protein to be the entry point of iron into the complex (Chahal and Outten 2012). Its histidine residue His-360 has been proposed to bind iron and together with Cys-405 of SufB take part in the cluster formation (Wada et al. 2009). The crystal structure of SufD from the SufBCD complex is depicted in **Figure 14**. The entire structure of the SufBCD complex is provided in **Figure 15**.

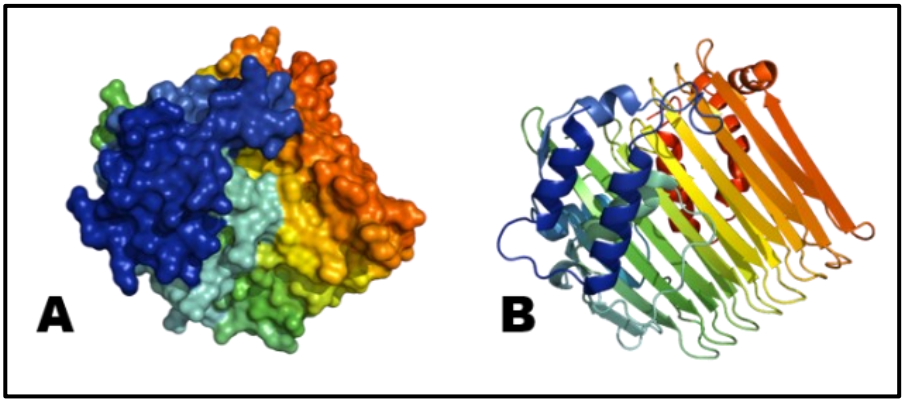

Figure 14: Crystal structure of SufD (PDB ID: 5AWF, Hirabayashi et al. 2015). The structure is homologous to that of SufB. **A** – surface model; **B** – ribbon model.

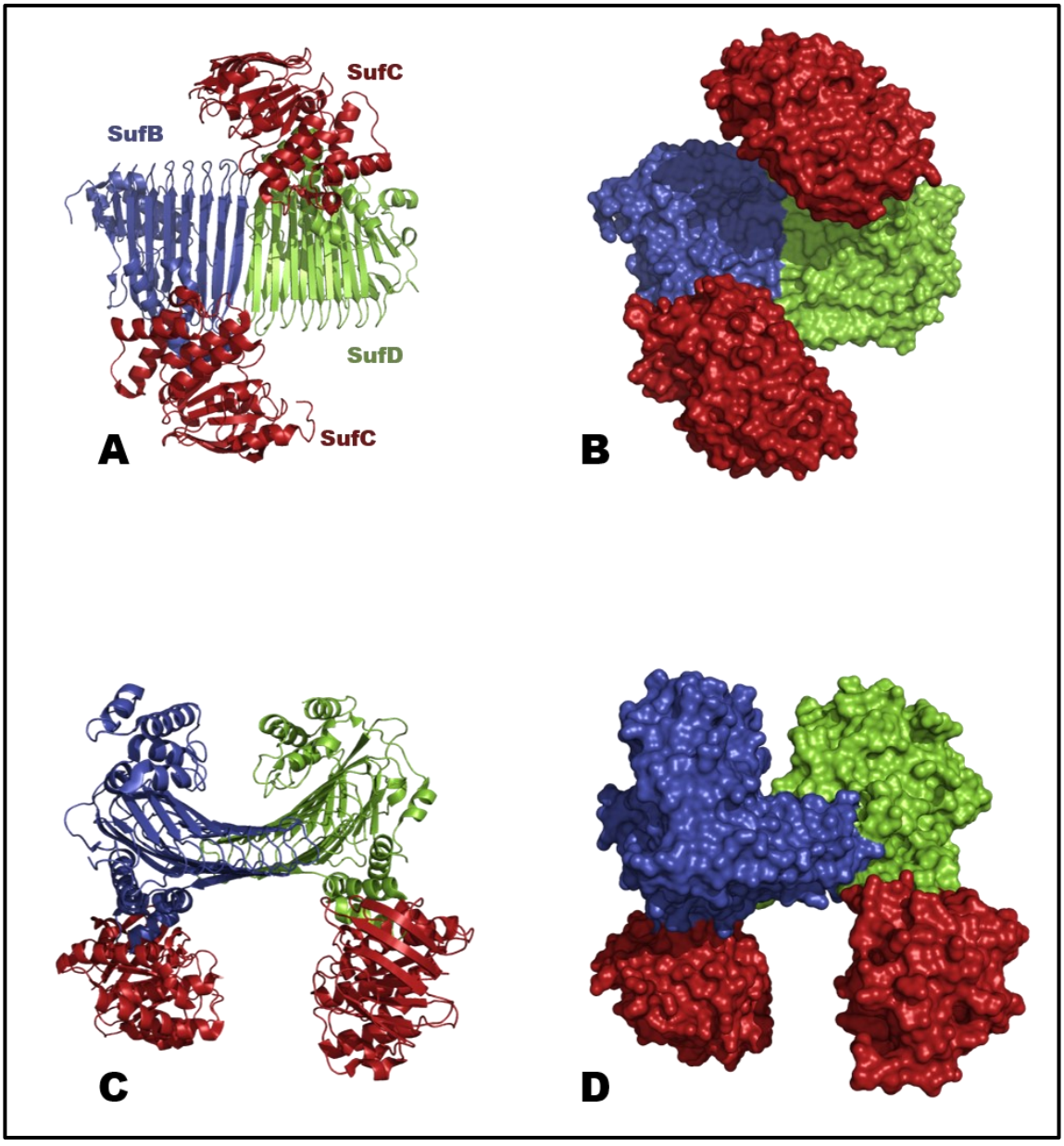

Figure 15: Crystal structure of SufBCD complex in a $SufBC_2D$ stoichiometry (PDB ID: 5AWF, Hirabayashi et al. 2015). **A**, **C** – ribbon model; **B**, **D** – surface model.

2.3.5.2.4 SufA

SufA is a member of the A-type iron-sulfur cluster carriers, which facilitates the transfer of FeS cluster to the recipient apoprotein (Gupta et al. 2009; Vinella et al. 2009). SufA has been proven to transfer its cluster to a wide range of proteins, including both [2Fe-2S] proteins (ferredoxin) and [4Fe-4S] proteins (biotin synthase, aconitase) (Gupta et al. 2009; Chahal and Outten 2012). SufA cannot transfer the cluster back to the SufBCD scaffold (Chahal et al. 2009). The crystal structure of SufA from *E coli* is shown in **Figure 16** (Wada et al. 2005).

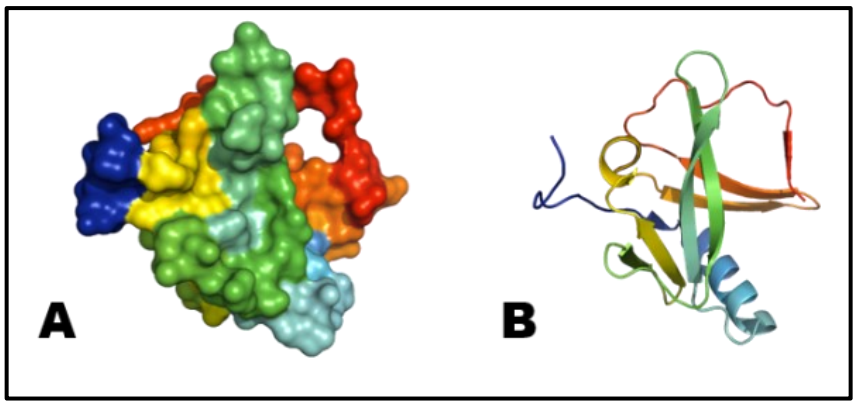

Figure 16: Crystal structure of SufA (PDB ID: 2D2A, Wada et al. 2005).
A – surface model; **B** – ribbon model.

2.3.5.3 SUF pathway in Preaxostyla

In *M. exilis* and *P. pyriformis*, homologues of 5 main proteins of the SUF pathway were identified, namely SufS, SufU, SufB, SufC, and SufD. Neither SufA nor SufE have been identified. The genome analysis provided some interesting features in gene composition, the most striking being the gene fusion of SufDSU (Vacek et al. 2018). Functional studies will be required to determine whether this fusion protein functions as a single unit, or whether it is working separately.

2.3.6 Iron-sulfur cluster synthesis in eukaryotic anaerobes and microaerophiles

Anaerobic lifestyle has led to many changes in the iron-sulfur cluster synthesis in single-cell eukaryotes. Although the main source of iron-sulfur clusters in the majority of sequenced eukaryotic organisms is provided by the ISC pathway, gene losses of ISC components are common, as well as the acquisitions of new genes via lateral gene transfers.

Common is the loss of parts of the late ISC. Namely, the loss of the IscA1-IscA2-Iba57 complex has been registered in *Encephalitozoon cuniculi* and *Trachipleistophora hominis* (Microsporidia) (Goldberg et al. 2008; Freibert et al. 2017). IscA2 and Iba57 have been also reported missing in *Giardia intestinalis* (Jedelský et al. 2011) and *Trichomonas vaginalis* (Schneider et al. 2011). The aforementioned enzymes are part of the late ISC, which maturates [4Fe-4S] enzymes. In mitochondria, these enzymes take part in oxidative phosphorylation and the TCA cycle, which anaerobes lack (Tachezy 2019). Therefore, it makes sense that the late ISC may have been lost in these organisms. Atm1 has been identified to take part in the transfer of a sulfur-containing compound from the ISC pathway in mitochondria to the CIA pathway in the cytosol. This protein has not been identified in any organism belonging in the group Metamonada (e. g. *T. vaginalis* Carlton et al. 2007; Schneider et al. 2011) and *G. intestinalis* (Pyrih et al. 2016). Atm1 was probably lost by the common ancestor of metamonads. How exactly does the ISC pathway of these organisms communicate with the CIA pathway is yet to be clarified. In *G. intestinalis,* dually localized components of the CIA pathway, Cia2, and Nbp35 have been proposed to take part in the transfer (Pyrih et al. 2016). Other proteins commonly missing in anaerobes and microaerophiles are parts of the CIA pathway. Dre2, which is part of an electron transport chain associated with the CIA scaffold, is missing in all sequenced anaerobes. The second part of this electron transport chain, Tah18, is missing in all metamonads (Carlton et al. 2007; Karnkowska et al. 2016; Pyrih et al. 2016; Vacek et al. 2018). This electron transport chain could either be replaced by an alternative source of electrons, or the electron transport chain might not be required at all in these organisms if the compounds used for synthesis by CIA do not need reduction.

A significant percentage of genes in most protists have been gained by a process called lateral gene transfer (LGT). LGT is the hand-over of genetic material between organisms that are not directly related (Sieber, Bromley, and Dunning Hotopp 2017). Amongst other genes, some single-cell eukaryotes gained parts of pathways for the iron-sulfur cluster synthesis from bacteria. The genes acquired in this process can function as an accessory to the canonical ISC, but in some cases, the acquisition of alternative pathways lead to a further reduction or loss of the ISC. The most extreme example of this process is the subject of this thesis, *M. exilis,* which acquired an almost complete SUF pathway via LGT from bacteria (Vacek et al. 2018). Since a related protist *P. pyriformis* also contains a SUF pathway, lacks the ISC, but contains an MRO, the acquisition of the SUF pathway likely led first to the loss of ISC, followed by the loss of mitochondria.

Another example of a pathway acquired by LGT is a microaerophilic flagellate from marine sediments called *Pygsuia biforma,* which also lacks an ISC pathway, which has been replaced by the SUF pathway (Stairs et al. 2014). Moreover, only a minimal SUF pathway has been identified in *P. biforma*, namely a fusion protein SufBC and the cell seems to completely lack a cysteine desulfurase. This suggests that the iron-sulfur cluster assembly in *P. biforma* might not be cysteine-dependent, similar to some Archaea, which inhabit a similar environment (Liu et al. 2010). The sufBC fusion gene has been found in two other organisms, the human parasite *Blastocystis hominis* and the marine anaerobe *Stygiella incancerata* (Denoeud et al. 2011; Tsaousis et al. 2012; Leger et al. 2016). Phylogenetic analyses showed that sufBC fusion genes from all three organisms cluster together forming a strongly supported clade with a sister group in *Methanomicrobiales* Archaea, supporting the theory that this protein has been acquired via LGT from Archaea. Interestingly, these three organisms are not closely related, and so the acquisition of SufBC either happened as three separate events, or the acquired gene has been passed on via LGT between eukaryotes in the same habitat. The LGT from methanogenic Archaea to *P. biforma* and *S. incancerata* does not seem improbable given their natural habitat in hypoxic sediment (Hamann et al. 2016; Leger et al. 2016). However, in the case of the human gut parasite *B. hominis,* this event is hard to imagine, even though this parasite does produce cysts which are released to the outside environment (Stenzel and Boreham 1996).

Apart from the SUF pathway, eukaryotes with components of the NIF pathway have also been identified. Namely the human intestinal parasite *Entamoeba histolytica* and its free-living relative, *Mastigamoeba balamuthi.* Both organisms have lost the ISC pathway and the main provider of iron-sulfur clusters is the NIF pathway. In the case of *M. balamuthi*, dual localization of the pathway in the mitosome, as well as the cytosol, has been confirmed experimentally (Nývltová et al. 2013). The dual localization of *E. histolytica* NIF has been speculated but not yet confirmed (Ali et al. 2004; Mi-ichi et al. 2009; Doležal et al. 2010).

3 Aims of the thesis

The aims of the thesis were to

1) Prepare a recombinant version of *M. exilis* SufC, the putative ATPase of the SUF system, in a native state.

2) Localize the SUF pathway in the cells of *M. exilis* and *P. pyriformis* by immunofluorescence.

3) Measure the ATPase activity of SufC and standardize the conditions for its activity.

4) Prepare a recombinant version of *M. exilis* SUF pathway scaffold protein SufB by co-expression with SufC.

5) Characterize the interaction between SufC and SufB proteins *in vitro.*

4 Materials and methods

4.1 Organisms and their cultivation

4.1.1 *Monocercomonoides exilis*

4.1.1.1 Cultivation

Monocercomonoides exilis strain PA203 was isolated from the large intestine of *Chinchilla lanigera* and is currently kept in a polyxenic monoeukaryotic culture. For the purposes of this thesis, this strain was cultivated using TYSGM-9 media (Diamond 1982) and bacterized with *Citrobacter freundii*. The culture was subcultured approximately every 5 days by the addition of 1 ml of well-grown inoculum into 10 ml of bacterized media. The culture was allowed to grow in 15 ml plastic air-tight tubes at 37°C. Bacterization of media was accomplished by inoculating one drop of *C. freundii* culture into fresh TYSGM-9 media and growing the bacteria at 37°C for 1-5 days.

For most experiments, it was necessary to upscale the initial culture to a larger volume to maximize the number of cells and minimize cell loss during filtration. The inoculation procedure is presented in **Table 1**. A single 10 ml culture can upscale to up to 2.8 l of culture. Times of growth are approximate and were altered according to the growth rate of the culture. The ideal cell concentration of the inoculum was taken as 1.5-3x10^5 cells/ml.

Table 1: Inoculation scheme for upscaling *M. exilis* PA203 culture.

Total volume of culture (ml)	Volume of inoculum (ml)	Volume of bacterized media (ml)	Approximate time of culture (hours)
10	1	9	72
45	5	40	72
175	45	130	24
675	175	500	24
1400	675	700	24

4.1.1.2 Culture filtration

Before using the culture for slide preparation and other experiments, it was necessary to minimise the number of bacteria. All cultures were first passed through a filter paper to remove larger clumps of bacteria and ensure faster filtration in the next step. The flow-through was then filtered through a polycarbonate membrane with a pore size of 3 μm (Whatman). This pore size ensured the bacteria pass through leaving the larger eukaryotic cells on top. To speed up the process, mild pressure was applied by 3ml plastic Pasteur pipettes. The cells were then washed twice by 250 ml of serum-free TYSGM media. The

supernatant was allowed to pass through the membrane until there was only a small amount on top of it left (approx. 20 ml). The filtered culture was observed under a light microscope to assess the number of cells and purity of the resulting culture. Ultimately, the culture was harvested from the top of the filter into 50ml tubes and centrifuged at 1200g for 10 min to obtain the cells in a pellet.

4.1.1.3 TYSGM-9 media preparation

All components listed in **Table 2** (except for bovine serum) were dissolved in distilled water and the pH was brought to 7.0-7.2. Inactivated bovine serum was added after sterilization by autoclaving and the medium was stored at 4°C before use.

Table 2: Composition of TYSGM-9 media.

Tryptone	0.2 % (w/v)
Yeast extract	0.1 % (w/v)
K_2HPO_4	16 mM
KH_2PO_4	3 mM
NaCl	130 mM
Heat-inactivated bovine serum (Gibco)	3 % (v/v)

4.1.2 Paratrimastix pyriformis

4.1.2.1 Cultivation

Paratrimastix pyriformis strain RCP-MX, ATCC 50935 was isolated from a swampy area in Rock Creek Park, Rockville, Maryland, USA (8th November 1995) and was cultivated in ATCC 802 media bacterized with an admixture of unspecified bacteria. 10 ml of bacterized media was inoculated with 1 ml of inoculum once a week. To obtain larger volumes, 5 ml of culture were inoculated into 40 ml of bacterized media. After 4 days, this volume could be inoculated into a larger volume of bacterized media to reach 1 l of culture.

4.1.2.2 Culture filtration

Similarly to *M. exilis*, all *P. pyriformis* cultures were filtered before obtaining slides and cell lysates. The procedure is identical to the one described previously in section 4.1.1.2, with the difference in the washing step, where 3% (v/v) LB media was used instead of TYSGM-9 media.

4.1.2.3 ATCC 802 media preparation

Cerophyll was added to distilled water, boiled for 5 minutes, and filtered through a filter paper. The volume was adjusted to compensate for evaporation and Na_2HPO_4 was added.

The media was sterilized by autoclaving and stored at 4°C before use. Concentrations of all components are listed in **Table 3**.

Table 3: Composition of ATCC 802 media.

Cerophyll (Cereal Grass Media, Ward's Science)	0.25 % (w/v)
Na_2HPO_4	3.5 mM

4.1.3 Trichomonas vaginalis

Trichomonas vaginalis strain TvT1 was used as a control for antibody specificity during immunofluorescence experiments. Cells transfected with TagVag2 vector (Hrdý et al. 2004) containing a SufC gene from *M. exilis* tagged with C-terminal 2x HA-tag were used. The cells were cultivated using TYM media (Diamond 1957) with selection antibiotic G418 (geneticin, ZellBio GmbH) in 200 mg/ml concentration. The cultures were grown at 37°C in 10ml glass tubes and inoculated once a day.

4.1.3.1 TYM media preparation

All components listed in **Table 4** except horse serum were dissolved in distilled water and the pH was altered to 6.2. Horse serum was added after the media was sterilized by autoclaving. The finished media was stored at 4°C before use.

Table 4: Composition of Diamond's TYM media.

Tryptone	2 % (w/v)
Yeast extract	1 % (w/v)
Maltose	0.5 % (w/v)
K_2HPO_4	6 mM
KH_2PO_4	5 mM
L-cysteine	8.25 mM
Ascorbic acid	1.13 mM
Ammonium Ferric (III) Citrate	0.9 mM
Inactivated horse serum (Gibco)	1 % (w/v)

4.1.4 Escherichia coli

Two strains of *Escherichia coli* were used, TOP10 (ThermoFisher Scientific) for plasmid amplification and Rosetta2 (Merck) for protein expression. These competent cells are lysogens of a bacteriophage DE3 and therefore carry a chromosomal copy of a T7 RNA polymerase under control of a lac promoter, which makes them suitable for protein expression induced by lactose or its synthetic analogue IPTG. Rosetta2 cells aid the expression of eukaryotic proteins that contain codons rarely used in *E. coli* by providing tRNAs for seven of these rare codons on a pRARE2 plasmid. This plasmid bears a

chloramphenicol resistance gene. Rosetta2 cells were selected using chloramphenicol (30 µg/ml) on top of the selection antibiotic of the expression vector.

Chemically competent *E. coli* was transformed using the heat shock method. Plasmid DNA (approximately 200 ng) or ligation mixture was added to 50 µl of competent cells on ice. After 20 minutes on ice, the tubes with cell-plasmid mixtures were placed in a heat block at 42°C for 45 seconds and immediately returned on ice to recover for 2 minutes. 500 µl of SOC medium was added to the cells and the culture was incubated on a shaker at 220 rpm and 37°C for 1 hour. The culture was plated onto LB agar plates with the appropriate drug resistance and grown overnight at 37°C.

4.1.4.1 LB media preparation

Liquid LB

LB broth (**Table 5**) was dissolved in distilled water and sterilized by autoclaving.

Table 5: Liquid LB media composition.

LB broth (Sigma)	2 % (w/v)

LB plates

All compounds (**Table 6**) were dissolved in distilled water and sterilized by autoclaving. The warm medium was then poured into sterile Petri dishes (approx. 30 ml per dish) inside the laminar box and left to cool.

Table 6: Media composition for LB plates.

LB broth (Sigma)	2 % (w/v)
Agar	1.5 % (w/v)

4.1.4.2 SOC media preparation

The composition of SOC media is listed in **Table 7**. Tryptone, yeast extract, NaCl, and KCl were dissolved in distilled water. The pH was brought to 7.0. Glucose and $MgCl_2$ were added from stocks under sterile conditions after the media was autoclaved. The media was kept at 4°C before use.

Table 7: SOC medium composition.

Tryptone	2 % (w/v)
Yeast extract	0.5 % (w/v)
NaCl	10 mM
KCl	2.5 mM
Glucose	0.3 % (w/v)
$MgCl_2$	10 mM

4.2 Gene cloning and protein expression

4.2.1 Gene amplification

SufB and SufC were amplified by PCR from cDNA using Primestar MAX DNA polymerase (Takara Bio). Primer sequences with restriction sites (in bold text) for cloning in different plasmids are listed in **Tables 8** and **9**. PCR conditions are listed in **Tables 10** and **11**. Primers with restriction sites were designed using Geneious software (Biomatters) and synthesized by KRD. The PCR products were visualized on 1% (w/v) TAE/agarose gels stained with SYBR safe (0.1% (v/v)), gel extracted and cleaned using NucleoSpin gel and PCR clean-up (Macherey-Nagel) kit according to manufacturer's protocol.

Table 8: Primer sequences with restriction sites for amplification of SufC and insertion into pET30a vector.

SufC, pET30a	
forward, **BamHI**	5'-TCATCT**GGATCC**CAAACTCAAAAGCCCCTT-3'
reverse, **SacI**	5'-TCATCT**GAGCTC**TTAAATCTTCACAACTCCCTCTG-3'

Table 9: Primer sequences with restriction sites for amplification of SufB and SufC and insertion into a pETDuet-1 vector.

SufB and SufC, pETDuet-1	
SufB, forward, **AscI**	5'-TCATCT**GGCGCGCC**TACTGCTTCATCTAAACCTTCAAGT-3'
SufB, reverse, **SalI**	5'-TCATCT**GTCGAC**CTAACCAACCGAGCCTTCCA-3'
SufC, forward, **FseI**	5'TCATCT**GGCCGG**CCATCAAACTCAAAAGCCCCTTTTAG-3'
SufC, reverse, **AatI**	5'-TCATCT**GACGTC**AATCTTCACAACTCCCTCTG-3'

Table 10: Conditions for amplification of SufC using Q5 polymerase for insertion into pET30a plasmid.

Number of cycles	**1x**	**35x**			**1x**	
Temperature	98°C	98°C	60°C	72°C	72°C	4°C
Time	30 s	10 s	30 s	45 s	5 min	∞

Table 11: Conditions for amplification of SufB and SufC using Primestar MAX polymerase for insertion into a pETDuet-1 plasmid.

Number of cycles	**1x**	**30x**			**1x**
Temperature	98°C	98°C	63°C	72°C	12°C
Time	10 s	5 s	3 s	8 s	∞

To maximize DNA yield for cloning into expression vectors, cleaned PCR products were cloned into pJET1.2/blunt PCR product amplification vector using a cloneJET PCR cloning kit (ThermoFisher Scientific, **Figure 17**). Ligation was carried out according to the manufacturer's protocol and was dependent on PCR product size and concentration. The ligation mixture was transformed into TOP10 competent cells.

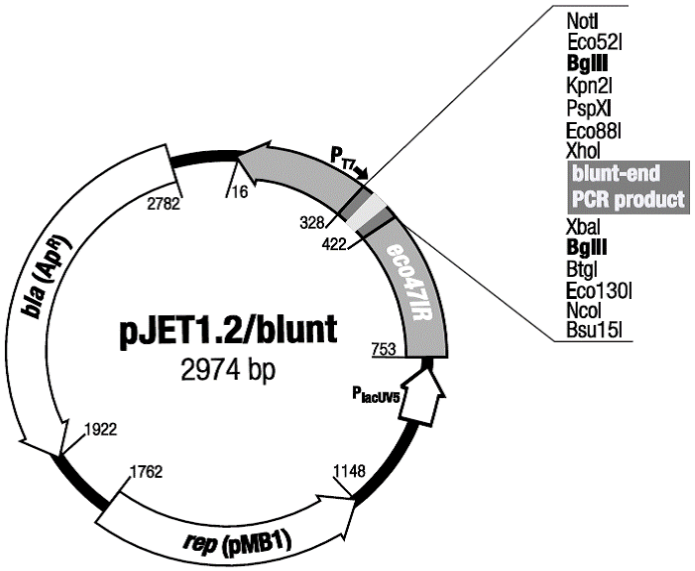

Figure 17: pJET1.2/blunt vector map. This vector was used for blunt-end PCR product cloning (CloneJET PCR Cloning Kit, ThermoFisher Scientific).

4.2.2 Expression vector preparation

For the expression of SufC, a commercially available expression vector pET30a (Novagen) was used. This vector contains a 6x His-tag (C-terminal and N-terminal), an S-tag (N-terminal), and a gene for kanamycin resistance (**Figure 18**). The co-expression of SufB and SufC was carried out using pETDuet-1 vector (Novagen), which bears two multiple cloning sites (MCS) (**Figure 19**). MCS1 is equipped with a 6x His-tag (N-terminal) and MCS2 with an S-tag (C-terminal). A 6x HA-tag was amplified from a p2623 plasmid (Kelly et al. 2007) and substituted the S-tag using XhoI and PacI restriction sites. pETDuet-1 has a gene for ampicillin resistance.

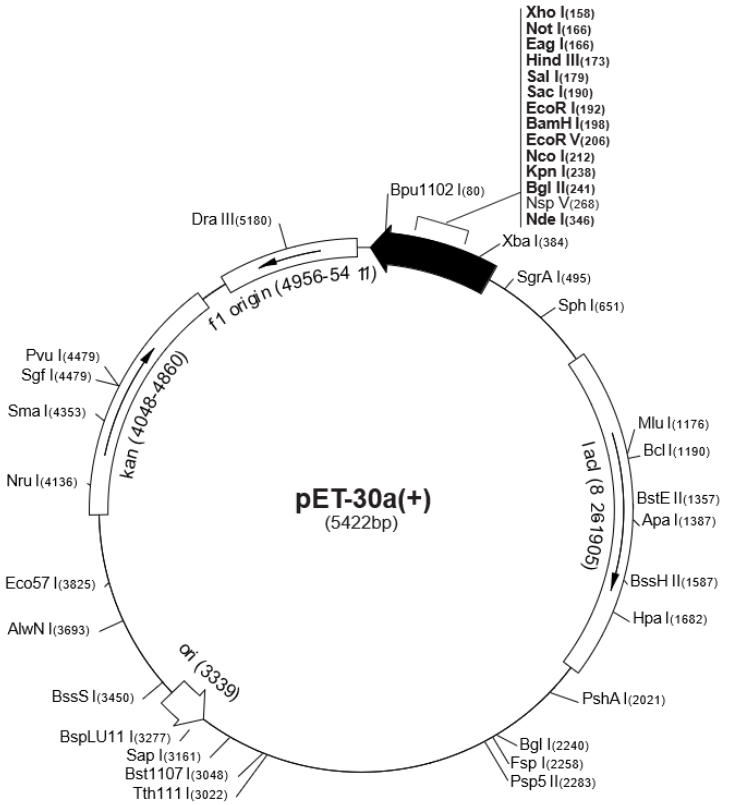

Figure 18: Restriction map of pET30a vector (Novagen). SufC (804 bp) was cloned into BamHI and SacI restriction sites.

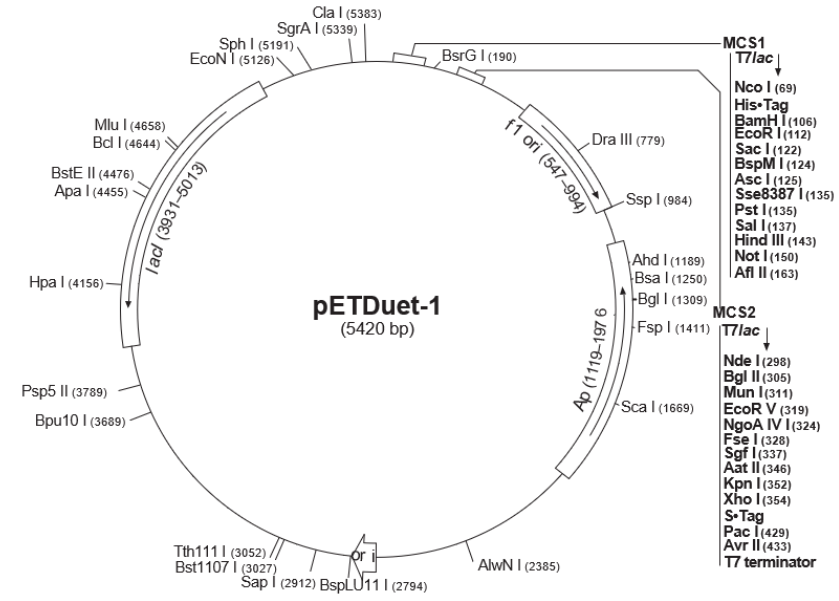

Figure 19: Restriction map of pETDuet-1 vector (Novagen). HA-tag was cloned between XhoI and PacI sites. SufB (1500 bp) was cloned into AscI and SalI sites and SufC (804 bp) was cloned using FseI and AatII sites.

Expression vectors and pJET constructs bearing the genes of interest were digested using restriction endonucleases. For cloning into pET30a, SufC and the vector were digested using BamHI and SacI (FastDigest ThermoFisher Scientific). For cloning into pETDuet-1, SufB was cloned first inco MCS1 using AscI and SalI, and later SufC was cloned into MSC2, using FseI and AatI (NEB). Reaction components for enzyme digests are listed in **Table 12**. All reactions were incubated at 37°C for 1 hour. DNA from the reactions was then separated on 1% (w/v) agarose gel. Digested vector and insert DNA were cut out of the gel and isolated using NucleoSpin gel and PCR clean-up kit (Macherey-Nagel).

Table 12: Double digest reaction components. The reaction was carried out in a 20 µl final volume.

DNA	1 µg
10x FastDigest Green Buffer	2 µl
Restriction enzyme 1	1 µl
Restriction enzyme 2	1 µl
dH_2O, nuclease-free	up to 20 µl

Digested vector and inserts were ligated using T4 DNA ligase (ThermoFisher Scientific). For pET30a, a molar ratio 3:1 insert:vector was used. Ligations of pETDuet-1 were performed at a 10:1 insert:vector molar ratio. The reaction was carried out at 16°C overnight. The ligation mixture was subsequently transformed into TOP10 competent cells.

Isolated minipreparations of DNA were analyzed by control restriction enzyme digestion under previously described conditions and further verified by Sanger sequencing using commercially available sequencing primers.

4.2.3 Protein expression

Protein expression was carried out using autoinduction according to Studier (Studier 2005) in Rossetta2 *E. coli* expression cell line. Expression constructs were transformed into competent cells, which were then grown on LB agar plates with kanamycin (50 µg/ml) in the case of pET30a, or ampicillin (100 µg/ml) in the case of pETDuet-1, both in presence of chloramphenicol (30 µg/ml). The plates were incubated overnight at 37°C and the next morning a single fresh colony was inoculated into 5 ml liquid LB (with antibiotics). This culture was grown on a shaker at 220 rpm and 37°C for 8 hours. After 8 hours, a second 5 ml LB culture (with antibiotics) was set up with 1:100 dilution of the previous culture. This culture was grown overnight at 220 rpm and 37°C. The next morning, a third 5 ml LB culture (with antibiotics) was set up using 1:100 dilution of the

overnight culture. This culture was also grown at 220 rpm and 37°C for 8 hours. After 8 hours, 10 ml MDG media (with antibiotics) was inoculated with a 1:50 dilution of the morning culture. The MDG culture was grown at 220 rpm, 37°C overnight. Autoinduction was set up using a 1:100 dilution of the MDG culture in 800 ml of ZYM-5052 media (with antibiotics). The culture was incubated at 28°C for 26 hours. Optical density was checked regularly. After 26 hours the culture was centrifuged at 4 000g for 10 minutes. The pellet was flash-frozen in liquid nitrogen and stored at -80°C for a limited amount of time before protein purification.

4.2.3.1 Media preparation for autoinduction

All components of MDG media (minimal media) and ZYM-5052 media (**Tables 13** and **14**) were dissolved in distilled water except for glucose and aspartate, which were added at the moment of setting up the culture. The media were autoclaved and stored at room temperature.

Table 13: MDG (minimal) media composition.

Na_2HPO_4	25 mM
KH_2PO_4	25 mM
NH_4Cl	50 mM
Na_2SO_4	5 mM
$MgSO_4$	2 mM
Glucose	0.5 % (w/v)
Aspartate	0.25 % (w/v)

Table 14: ZYM – 5052 media composition.

Na_2HPO_4	25 mM
KH_2PO_4	25 mM
NH_4Cl	50 mM
Na_2SO_4	5 mM
$MgSO_4$	2 mM
Glucose	0.05 % (w/v)
Tryptone	1 % (w/v)
Yeast extract	0.5 % (w/v)
Lactose	0.2 % (w/v)
Glycerol	0.5 % (w/v)

4.2.4 Protein purification under native conditions

Both SufC alone and SufB co-expressed with SufC were purified using affinity chromatography with Ni-NTA agarose (ThermoFisher). The pellets were resuspended in 25 ml of purification buffer (**Table 15**) with complete protease inhibitor (Roche). Cells

were broken using French cell press (7 000-10 000 psi). The lysate was then centrifuged in an ultracentrifuge at 100 000g for 1 hour at 4°C. Pellet was separated from the supernatant (soluble fraction), which was used for purification of the protein using Ni-NTA agarose under native conditions. Ni-NTA agarose was well mixed and 10 ml of slurry were poured into a 50ml affinity chromatography column (Bio-rad). The column was equilibrated with 50 ml of purification buffer. 10mM final concentration of imidazole was added to the soluble fraction to minimise unspecific proteins binding. The soluble fraction was added to the column, the column was capped on both ends and the mixture was incubated at 4°C for 1 hour in rotation. The caps were then removed from the column and the flow-through was collected. The column was washed once using 50 ml of purification buffer. A second wash was carried out with 50 ml of buffer + 30 mM imidazole. The protein was eluted in three elutions with buffer containing different amounts of imidazole. Elution 1 consisted of 10 ml of buffer +150 mM imidazole, Elution 2 with 5 ml of buffer +150 mM imidazole and Elution 3 using buffer + 300mM imidazole.

Table 15: Composition of the purification buffer.

HEPES-KOH pH 8.0	50 mM
NaCl	300 mM
Glycerol	10 % (v/v)
β-mercaptoethanol	10 mM

To eliminate imidazole from the protein samples the buffer was exchanged using Amicon 30 000 MWCO filters for imidazole-free buffer. The purification efficiency was assessed by SDS-page and western blot analyses.

4.3 SDS-PAGE

SDS-PAGE (sodium dodecyl sulfate-polyacrylamide gel electrophoresis) was used for the analysis of protein samples and further analysis by western blot. The polyacrylamide gels (12% acrylamide, 0,75 mm thick) were mixed and poured according to **Table 16**. The samples were mixed with sample buffer (**Table 17**) and incubated at 100°C for 5 minutes. Once the gels set, samples were loaded into the wells. Page Ruler Plus Prestained Protein Ladder (ThermoFisher Scientific) was used as a marker for size determination. Electrophoresis was carried out in 1x TGS buffer (Bio-Rad, **Table 18**), at a constant current of 25 mA per gel for approximately 45 minutes. For protein visualization, the

polyacrylamide gels were stained for 1 h with Coomassie Brilliant Blue stain (**Table 19**) and destained with a destaining solution (**Table 20**) until proteins were visible on the gel.

Table 16: Composition of running and stacking gel for SDS-PAGE.

Running gel		**Stacking gel**	
Tris-HCl, pH 8.8	375 mM	**Tris-HCl, pH 6.8**	125 mM
Acrylamide	12 % (w/v)	**Acrylamide**	4 % (w/v)
SDS	0.1 % (w/v)	**SDS**	0.1 % (w/v)
APS	0.1 % (w/v)	**APS**	0.1 % (w/v)
Temed	10 uL	**Temed**	10 uL

Table 17: 5x sample buffer for SDS-PAGE protein samples.

Tris-HCl, pH 8.8	200 mM
Glycerol	25 % (v/v)
bromophenol blue	1.5 mM
β-mercaptoethanol	710 mM

Table 18: Contents of 1x TGS buffer (Bio-Rad).

Tris-HCl, pH 8.3	25 mM
Glycine	129 mM
SDS	0.1 % (w/v)

Table 19: Contents of Coomassie Brilliant Blue stain.

Coomassie Brilliant Blue R-250 (Sigma)	0.1 % (w/v)
Methanol	50 % (v/v)
glacial acetic acid	10 % (v/v)

Table 20: Contents of destaining solution.

methanol	25 % (v/v)
glacial acetic acid	10 % (v/v)

4.4 Western blot

Western blot analysis was used for the detection of specific proteins in protein samples. Samples separated by SDS-PAGE were transferred from polyacrylamide gel to PVDF membrane (Amersham) by Trans-blot turbo transfer system (Bio-Rad). The membrane was activated in pure methanol for a few seconds prior to transfer. The gel, membrane and four pieces of filter paper were soaked in transfer buffer (**Table 21**) and assembled in a sandwich. The transfer was carried out for 30 minutes using a built-in protocol for mini format gels.

For blocking of non-specific antibody binding, the membrane was blocked with a blocking solution (**Table 22**) for 1 hour at room temperature. After blocking, the membrane was incubated with a primary antibody diluted in the blocking solution (dilution ratio depending on the antibody used) for 1 hour at room temperature. After that,

the membrane was washed with 0.1% PBS/Tween 20 3x for 10 minutes. An HRP (horseradish peroxidase)-conjugated secondary antibody (Sigma) at 1:2000 dilution in the blocking solution was added and the membrane was incubated for 1 hour at room temperature. Finally, the membrane was washed in 0.1% PBS/Tween 20 3x for 10 minutes.

The PVDF membrane was developed by chemiluminescence in Amersham Imager 600 (GE Healthcare) using Clarity Western ECL peroxidase substrate (Bio-Rad).

Table 21: Composition of western blot transfer buffer.

Trizma base	25 mM
Glycine	192 mM
SDS	0.25 % (w/v)
Methanol	20 % (v/v)

Table 22: Composition of the blocking solution, all components were dissolved in 1x PBS.

low fat dried milk	5 % (w/v)
Tween 20 (Sigma)	0.25 %

4.5 SufC antibody preparation and testing

Purified protein was delivered to the laboratory of prof. Roland Lill in Philips Universität Marburg for polyclonal antibody production in the rabbit. Immunized serum was then cleaned on affinity resin using purified SufC protein.

The antibody was tested using western blot analyses using the lysate of *M. exilis* and *P. pyriformis*. For more accurate results antibodies were also tested using immunoprecipitation on *M. exilis* lysate. Immunoprecipitation was carried out using Dynabeads G-protein coupled immunoprecipitation kit according to the manufacturer's procedure (ThermoFisher Scientific, USA). The resulting beads-antibody-antigen mixture was analysed using mass spectrometry in Biocev proteomics core facility.

4.6 Immunofluorescence slide preparation

Fluorescence slides were prepared following a protocol according to Dawson (Dawson et al. 2008). 250 ml cultures of *M. exilis* and *P. pyriformis* were filtered and the cells were washed. The cells were fixed by the addition of formaldehyde to a final concentration of 1% (v/v) and pelleted by centrifugation at 1200g for 10 minutes at 4°C. The pellet was washed by gently resuspending in 5 ml of 1x PEM buffer (**Table 23**) and centrifuged at 1200g for 10 minutes at 4°C. The supernatant was discarded and the cells were resuspended in 200 µl of 1x PEM buffer. To attach the cells to coverslips, poly-L-lysine

was used. Two coverslips were cleaned using ethanol and wiped dry with a paper tissue. 15 µl of poly-L-lysine was placed on one of the coverslips and both coverslips were rubbed together. Coverslips were then placed into a 6-well plate with the poly-L-lysine side facing upwards. 100 µl of cell suspension were pipetted on the polylysine coverslip. Using a pipette tip the suspension was spread and left to attach at room temperature for 30 minutes. The cells were then permeabilized with 1 ml of 0.1% (v/v) TritonX-100 in PEM buffer for 10 minutes. The slides were then washed 3 times with PEM buffer for 30 seconds. Non-specific binding was blocked by adding 1 ml of PEMBALG buffer (**Table 24**) and incubating for 30 minutes. Primary antibodies were diluted in 1 ml PEMBALG and slides were incubated for 2 hours at room temperature. The primary antibody was washed away three times in 1 ml of PEM buffer for 5, 10 and 15 minutes. AlexaFluor secondary antibodies (ThermoFisher scientific) were diluted in 1 ml of PEMBALG using a 1:1000 dilution. The slides were incubated for 1 hour at room temperature. After incubation, the secondary antibody was washed away using 1 ml of PEM buffer three times for 5, 10 and 15 minutes. The slides were then mounted using Vectashield mounting medium (Vector Laboratories, Inc.) with DAPI. For each slide, roughly 15 µl of mounting medium was used. Coverslip edges were then sealed using nail polish and the slides were stored at 4°C in the dark.

Table 23: Composition of 1x PEM buffer.

PIPES	100 mM
EGTA	1 mM
$MgSO_4$	0.1 mM

Table 24: Composition of 1x PEMBALG.

PIPES	100 mM
EGTA	1 mM
$MgSO_4$	0.1 mM
Lysine	100 mM
Cold water fish skin gelatin (Sigma)	0.5 % (w/v)

4.7 ATPase activity measurement

ATPase activity of SufC recombinant protein was measured using an ATP/NADH coupled spectrophotometry assay (**Figure 20**). This assay enables visualization of ATP hydrolysis by using phosphoenolpyruvate and two coupling enzymes, pyruvate kinase and L-lactate dehydrogenase, to detect the change of added NADH to NAD, which is equivalent to the change of ATP to ADP.

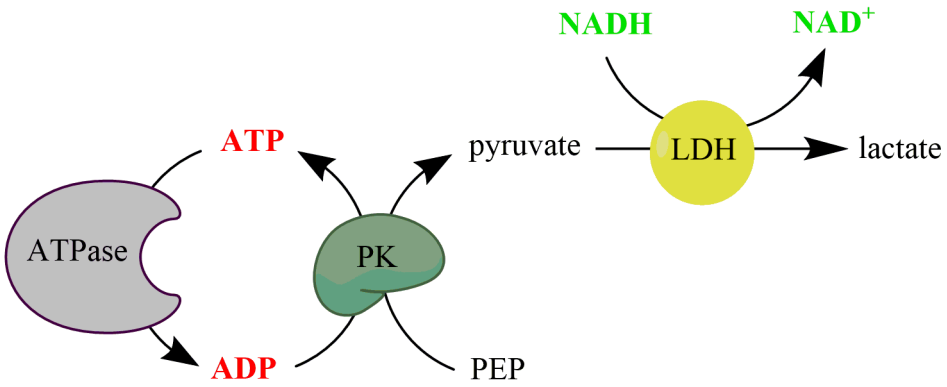

Figure 20: ATP/NADH coupled assay for ATPase activity measurement. **PK** – pyruvate kinase; **PEP** – phosphoenolpyruvate; **LDH** – L-lactate dehydrogenase.

The absorbance of NADH was measured using Shimadzu UV-2600 UV-Vis spectrophotometer and UVprobe software at 340 nm wavelength. All reactions were measured in quartz cuvettes with 1 ml volume and length of 1 cm for 5 minutes. Reaction components are specified in **Table 25**. The reactions were incubated at room temperature and started by the addition of ATP or SufC. To specify ideal conditions for SufC activity, the activity was measured in buffers of different range of pH, salt concentration and cofactor concentrations.

Table 25: Reaction components of ATPase activity measurement, the reaction was carried out in 1 ml total volume.

Phosphoenolpyruvate	4 mM
L-lactate dehydrogenase	20 U/ml
Pyruvate kinase	20 U/ml
NADH	0.2 mM
ATP	1 mM
SufC recombinant protein	5.7 µg/ml

The specific activity was calculated from ΔAbs (the change of absorbance) in the first 60 seconds after the reaction stabilized. The change of absorbance of NADH at 340 nm equals the amount of NAD produced which equals the amount of ATP hydrolysed to ADP. The concentration of hydrolyzed ATP was calculated from the following equation:

$$c = \frac{\frac{Abs_0 - Abs_t}{t}}{\varepsilon * l}$$

ε – extinction coefficient of NADH (ε = 6220 M^{-1} . cm^{-1})
l – cuvette width (l = 1 cm)
Abs_0 – starting absorbance
Abs_t – absorbance at time t
t – time (min)
c – concentration of ATP hydrolyzed by the enzyme (mmol/min/ml of enzyme)

Resulting concentration in mmol of hydrolyzed ATP/min/ml of the enzyme was then converted to µmol/min/ml (multiplied by 1000) and divided by the concentration of the enzyme in the reaction mixture (mg/ml) to get a specific activity (µmol of hydrolyzed ATP/min/mg of enzyme).

4.7.1 pH standardization

For the standardization of buffer pH, a poly buffer adjusted to different pHs in a range between 5-10 was used. Buffer composition and reaction components are listed in **Table 26**.

Table 26: Buffer composition for pH standardization

MES	25 mM
HEPES	25 mM
TRIS	25 mM
KCl	200 mM
$MgCl_2$	10 mM
DTT	1 mM

4.7.2 Ionic strength buffer standardization

For ionic strength standardization, a 50mM Tris-HCl pH 9.0 buffer was used. Buffer composition is listed below (**Table 27**), different concentrations in a range between 25-400mM NaCl and KCl were used.

Table 27: Buffer composition for salt standardization

Tris-HCl pH 9.0	50 mM
$MgCl_2$	10 mM
DTT	1 mM

4.7.3 Metal cofactor standardization

For metal cofactor standardization a 50mM Tris-HCl buffer pH 9.0, 50mM NaCl buffer was used (**Table 28**). $MgCl_2$ and $MnCl_2$ were tested in a concentration ranging between 1-10mM. $ZnSO_4$ and $CoCl_2$ were tested in three concentrations, 1mM, 2mM and 5mM.

Table 28: Buffer composition for metal cofactor standardization

Tris-HCl pH 9.0	50 mM
NaCl	50 mM
DTT	1 mM

4.8 Size exclusion chromatography

Size exclusion fast protein liquid chromatography (FPLC SEC) was used to analyze the size of putative complexes that may form between the co-expressed SufB and SufC. This procedure is used to separate proteins according to size. The protein mixture was first purified by affinity chromatography using Ni-NTA agarose. The analysis was performed using liquid chromatograph FPLC BioLogic DuoFlow (Bio-Rad) with UV-Vis detector (280 nm) by doc. RNDr. Ivan Hrdý, Ph.D. 500 µl of protein mixture was loaded onto Superdex 200 increase 10/300 GL column and 36 fractions (500 µl each) were collected. Chromatograms were created by the BioLogic DuoFlow software. Three runs were performed altogether with three elution buffers with slightly different compositions (**Tables 29-31**) to test whether the measured complexes were stable in increased salt concentration or with the addition of ATP. All buffers were filtered and degassed before use. All fractions were then analysed on SDS-PAGE.

Table 29: FPLC elution buffer 1

HEPES-KOH pH 8.0	50 mM
NaCl	300 mM
Glycerol	10 % (v/v)
β-mercaptoethanol	10 mM

Table 30: FPLC elution buffer 2

HEPES-KOH pH 8.0	50 mM
NaCl	1 M
Glycerol	10 % (v/v)
β-mercaptoethanol	10 mM

Table 31: FPLC elution buffer 3

HEPES-KOH pH 8.0	50 mM
NaCl	300 mM
ATP	1 mM
Glycerol	10 % (v/v)
β-mercaptoethanol	10 mM

To calculate the size of protein complexes present in each fraction, Bio-Rad gel filtration standards (**Table 32**) were run on the same column. The FPLC chromatograph of the standards with corresponding molecular weights may be seen in **Figure 21.** The calibration curve (**Figure 22**) was plotted using the gel-phase distribution coefficient (K_{AV}*) against the logarithmic function of the expected molecular size of each standard (logMW). The sizes of SufB and SufC eluted fractions were calculated from the linear regression equation of the calibration curve.

***$K_{AV} = (V_e - V_0)/(V_c - V_o)$**, where V_e= elution volume, V_o = void volume, V_c = bed volume (total volume of material in the column)

Table 32: Gel filtration standard components (Bio-Rad)

Component	Molecular weight (kDa)
Thyroglobulin (bovine)	670.00
γ-globulin (bovine)	158.00
Ovalbumin (chicken)	44.00
Myoglobin (horse)	17.00
Vitamin B12	1.35

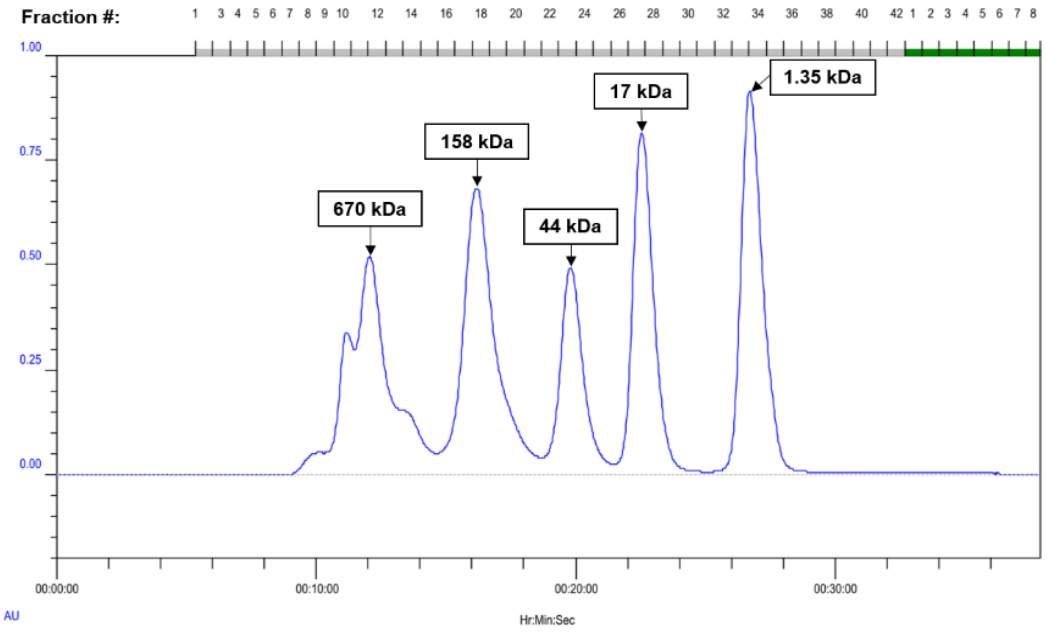

Figure 21: FPLC chromatograph of the SEC standards. Each peak represents a protein standard with its molecular weight in a box above it.

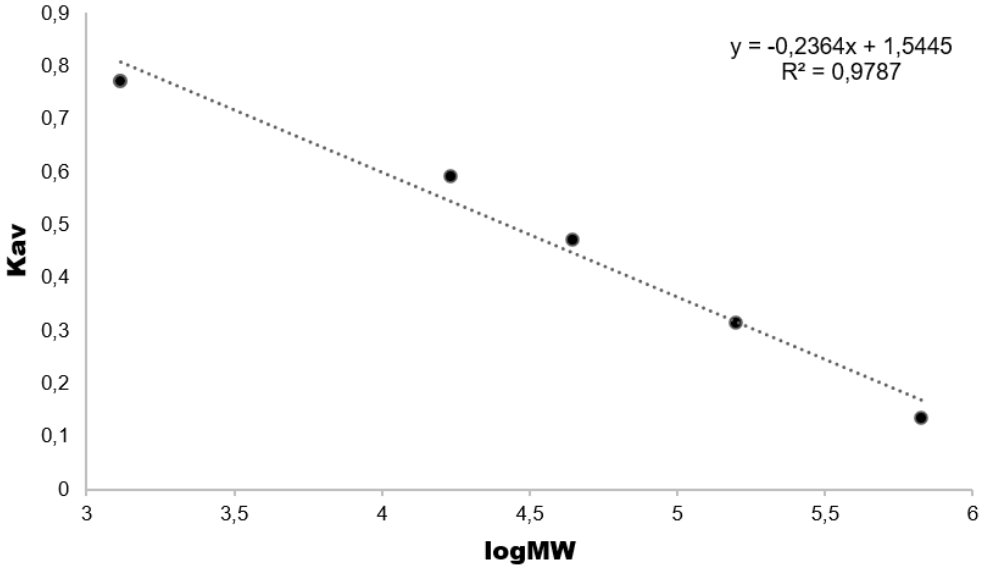

Figure 22: Calibration curve of Bio-Rad size exclusion chromatography standards. The graph shows a linear regression of gel-phase distribution coefficient plotted against logarithmic function of molecular weight of the standards. Sizes of SufB-SufC eluted fractions were calculated using the equation of linear regression.

5 Results

5.1 Isolation of recombinant SufC under native conditions

SufC was purified by affinity chromatography using Ni-NTA agarose. All fractions of purification were analyzed by SDS-page and western blot (**Figure 23**). The His-tagged protein displayed an approximate molecular weight of 40 kDa (marked by an arrow).

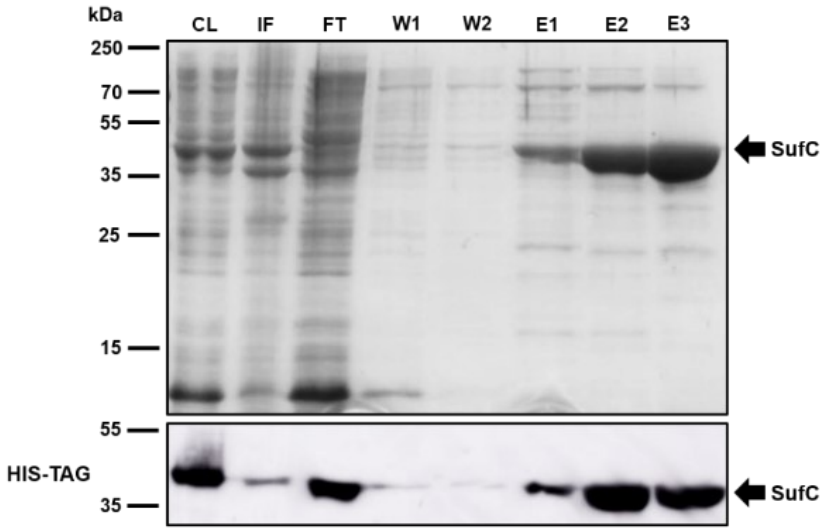

Figure 23: SufC purification fractions analyzed on SDS-PAGE stained by Coommassie briliant blue (top) and a western blot of the purification gel stained by an anti His-tag antibody (bottom). **CL** – cleared lysate; **IF** – insoluble fraction; **FT** – flow-through; **W1**, **W2** – wash 1 and 2; **E1**, **E2**, **E3** – elutions 1, 2 and 3.

5.2 SufC antibody testing

5.2.1 Western blot

Polyclonal antibody against purified SufC protein (produced in rabbit) was tested using western blot analysis. **Figure 24** shows the western blot, the antibody was tested on *M. exilis* and *P. pyriformis* cell lysates. The black arrow shows an approximate molecular weight of SufC. The antibody seems to detect an unspecific band around 100 kDa on *P. pyriformis* lysate and a faint band of correct molecular weight along with some unspecific bands in *M. exilis* lysate.

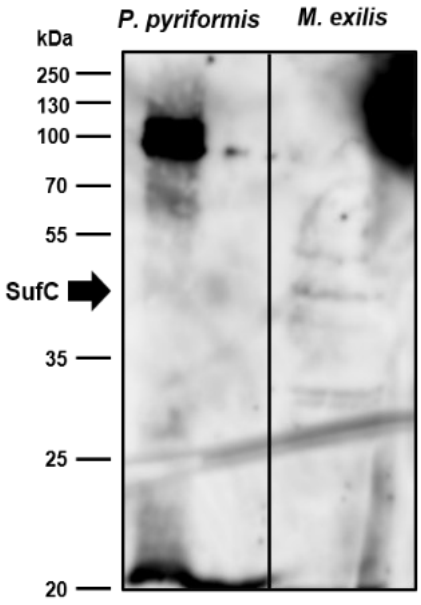

Figure 24 – Western blot testing SufC polyclonal antibody on *P. pyriformis* (left lane) and *M. exilis* (right lane) lysates. The arrow shows approximate molecular weight of SufC with a His-tag.

5.2.2 Immunoprecipitation

To confirm the affinity of the antibody to *M. exilis* SufC, immunoprecipitation of target antigens was performed using *M. exilis* cell lysate. Fold change represents the enrichment of the protein in the sample and was calculated by the proteomics core facility in Biocev, based on a negative control (*M. exilis* lysate without antibody). **Table 33** shows the Mass spectrometry analyses of the antigens bound to the anti SufC antibody.

Table 33: Mass spectrometry results of immunoprecipitation of *M. exilis* lysate using antibody against SufC. Protein hits are arranged base on occurrence in the sample, which is described by fold change (amount of protein present in the sample compared to the negative control).

Protein ID	Description	Expected MW (kDa)	Fold change
MONOS_7909	conventional actin	42.5	37.8
SufC_translation	SufC	29.4	8.2
MONOS_4852	Dpy-30 motif	54.9	6.8
MONOS_8492; 6335; 3652	P-type ATPase superfamily protein	126.8	3.5
MONOS_603	aspartate/ornithine carbamoyltransferase	45.0	2.2
MONOS_5230	protein kinase	10.7	2.2
MONOS_740	peroxiredoxin	19.1	1.8
MONOS_15594	actin-related protein 2	44.7	1.7
MONOS_1066	glutamine synthetase	49.4	1.6
MONOS_6009	GTP-binding protein-related isoform 1	40.9	1.6
MONOS_6123	aminoacyl-histidine dipeptidase	56.3	1.6
MONOS_14853	large subunit ribosomal protein L29e	18.6	1.5
MONOS_9439	Rab32A1	25.0	1.4
MONOS_231; 577; 871	Phosphoserine transaminase	43.9	1.4
MONOS_4780; 1296	Clan MH, family M20, peptidase T-like metallopeptidase	56.3	1.3
MONOS_2187;10869;10869	fructose bisphosphate aldolase	34.6	1.1
MONOS_199	Sly1	74.3	1.1
MONOS_14814	V-type proton ATPase subunit D	39.7	1.1
MONOS_1461; 10363	acetyl-CoA synthetase (ADP-forming)	77.9	1.0

5.3 Immunofluorescence

SufC antibody was used for *in situ* localization of SufC in cells using immunofluorescence. Permanent slides for immunofluorescence were viewed under Leica SP8 confocal microscope. *T. vaginalis* cells transfected with the SufC gene tagged with an HA-tag were used as a control of SufC antibody specificity. Figure 22 shows pictures of a *T. vaginalis* cell stained with anti SufC (1:500 dilution) and anti HA-tag (1:100 dilution) antibodies. The primary antibodies were visualized using AlexaFluor 488 and AlexaFluor 594 secondary antibodies (1:1000 dilution), respectively. Panel A shows anti SufC antibody signal and panel B displays anti HA-tag antibody signal (**Figure 25**).

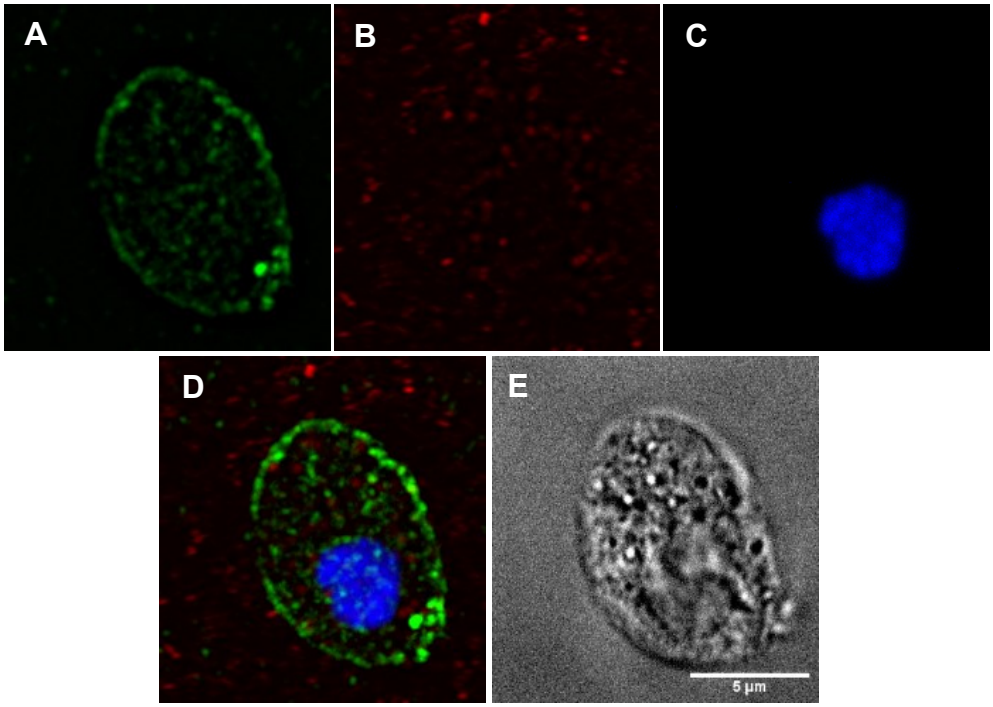

Figure 25: Immunoflurescence assay of *T. vaginalis* expressing *M. exilis* SufC. **A** – SufC, rabbit primary anti SufC antibody in a 1:500 dilution and secondary AlexaFluor 488 antibody in a 1:1000 dilution; **B** – anti HA-tag primary antibody + AlexaFluor 594 secondary antibody (both 1:1000), **C –** nucleus stained with DAPI (VectaShield mounting medium), **D** – merge of A, B and C; **E** – bright field image of the cell

The anti SufC antibody was used for localisation of SufC in *M. exilis* and *P. pyriformis.* **Figures 26** and **27** show *M. exilis* and *P. pyriformis* cells (only partially preserved in case of *M. exilis*) stained with anti SufC primary antibody (1:500) and secondary AlexaFluor 488 in a 1:1000 dilution.

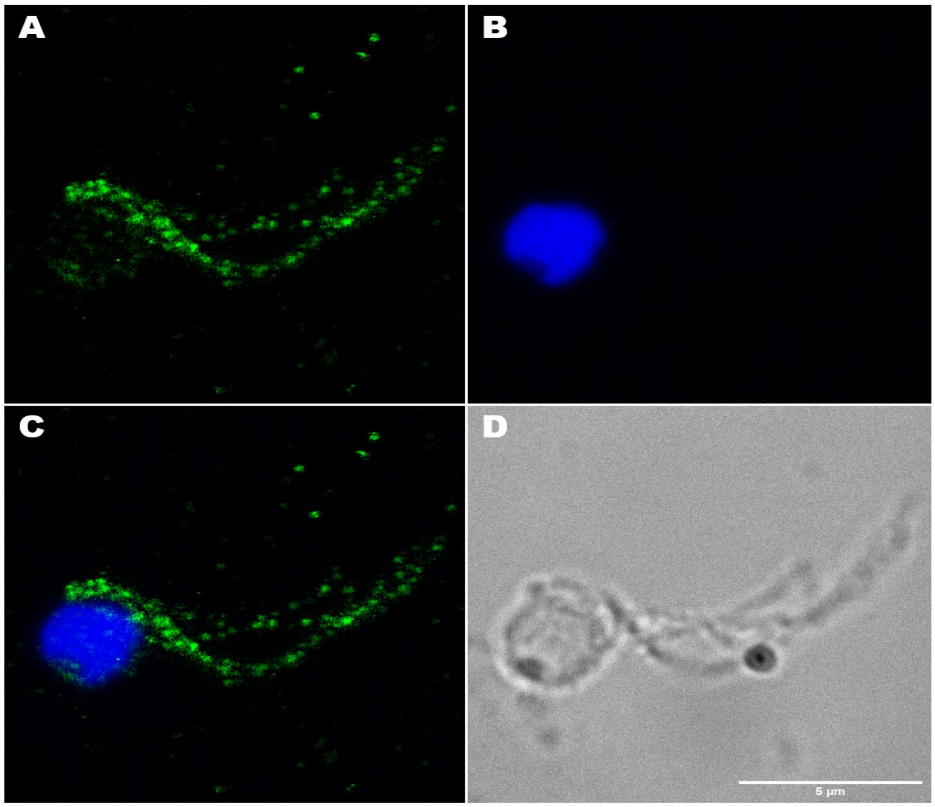

Figure 26: Immunoflurescence assay of SufC in a cell of *M. exilis*. **A** – SufC, primary anti SufC antibody in a 1:500 dilution and secondary AlexaFluor 488 antibody in a 1:1000 dilution; **B** – nucleus stained with DAPI (VectaShield mounting medium); **C** – merge of A and B; **D** – bright field image.

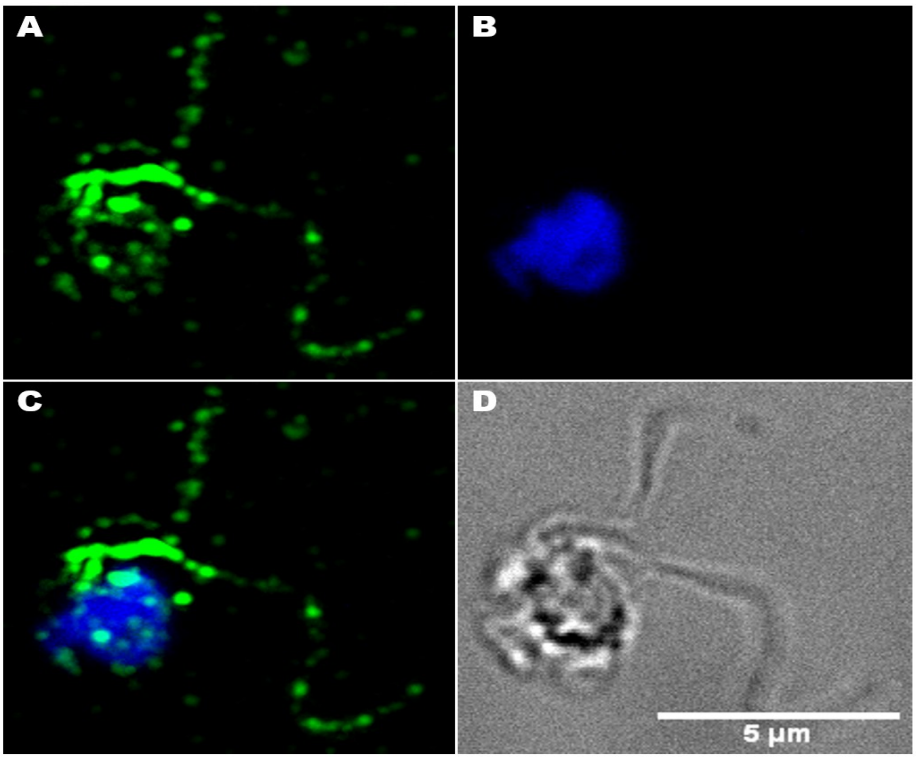

Figure 27 Immunoflurescence assay of SufC in a cell of *P. pyriformis*. **A** – SufC, primary anti SufC antibody in a 1:500 dilution and secondary AlexaFluor 488 antibody in a 1:1000 dilution; **B** – nucleus stained with DAPI (VectaShield mounting medium); **C** – merge of A and B; **D** – bright field image of the cell.

5.4 SufC activity

The ATPase activity of SufC was measured using an NADH-coupled spectrophotometric assay. To standardize the ideal conditions for the enzyme, the activity was measured in different ranges of pH, salt concentrations and different metal cofactors.

5.4.1 pH standardization

All reactions for standardization of pH were initialized by the addition of SufC. However, this way the activity of the enzyme took too long to become stable, therefore in all other instances, reactions were initialized by the addition of ATP. **Figure 28** shows the specific activity of SufC in different pHs of the reaction buffer. The curve shows an average of three independent measurements. All graphs were processed using GraphPad Prism software. From this graph, an ideal pH for activity was determined as pH 9.0.

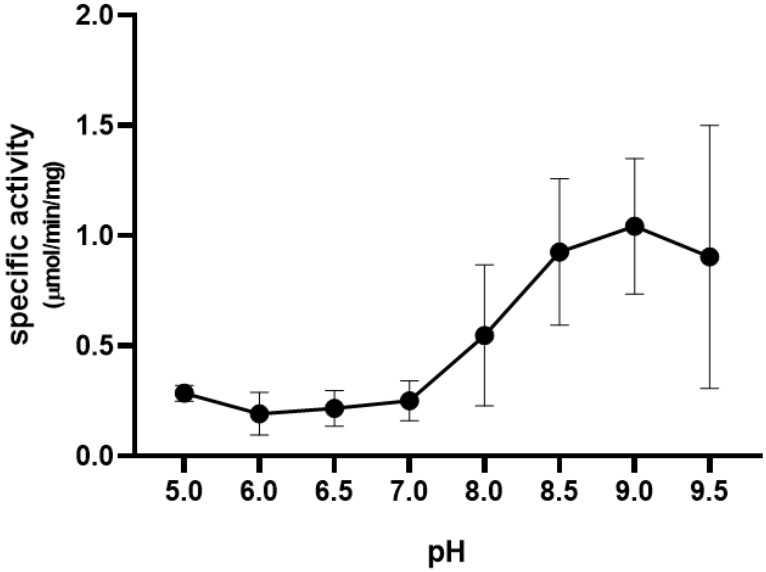

Figure 28: Specific ATPase activity of SufC based on pH of the reaction buffer. Graph shows an average of three independent measurements, error bars show standard deviation calculated by GraphPad Prism software.

5.4.2 Ionic strength buffer standardization

The reactions were measured in different concentrations of KCl or NaCl ranging from 25-400mM. The enzyme was active in all measured concentrations of salts. Activities measured in different concentrations of KCl showed no trend in the change of activity. In the case of NaCl, activity peaked at 50 mM concentration. 50 mM NaCl was therefore

determined as the ideal salt and its concentration. **Figures 29** and **30** show graphs of specific activities of SufC based on the concentration of NaCl and KCl, respectively.

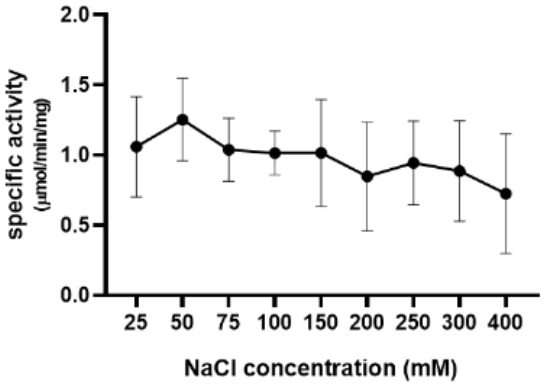

Figure 29: Specific initial activity of SufC based on concentration of NaCl. Graph shows an average of three independent measurements, error bars indicate standard deviation calculated by GraphPad Prism software.

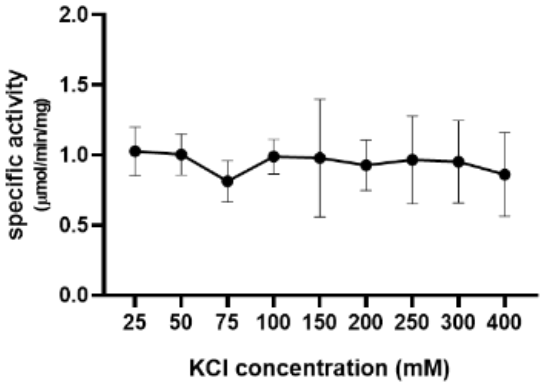

Figure 30: Specific initial activity of SufC based on concentration of KCl. Graph shows an average of three independent measurements, error bars indicate standard deviation calculated by GraphPad Prism software.

5.4.3 Metal cofactor standardization

The activity was measured in the presence of $MgCl_2$, $MnCl_2$, $ZnSO_4$, and $CoCl_2$. No activity was measured in the presence of $CoCl_2$, and $ZnSO_4$ caused the enzyme to precipitate. The enzyme showed some activity with lower concentrations of $MnCl_2$, however, when the concentration was increased over 4 mM, a precipitate was observed in the solution resulting in an increase of the absorbance (**Figure 31**). In the presence of $MgCl_2$, the enzyme was active in all concentrations of the compound, showing no significant change above 4 mM concentration (**Figure 32**). The specific activity (concentration of hydrolyzed ATP per minute per mg of purified SufC) measured at pH 9.0, 50 mM NaCl and 8 mM $MgCl_2$ was 1.18 µmol/min/mg (an average of three independent measurements with a standard deviation 0.09).

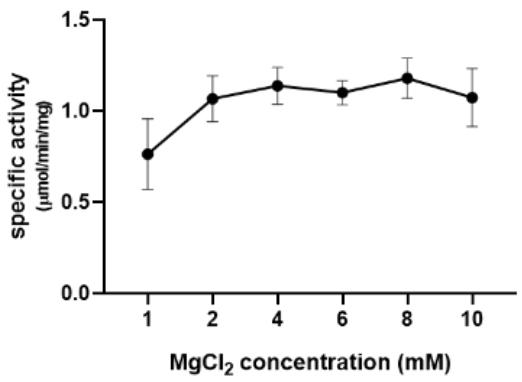

Figure 31: Specific initial activity of SufC based on concentration of $MgCl_2$. Graph shows an average of three independent measurements. error bars indicate standard deviation calculated by GraphPad Prism software.

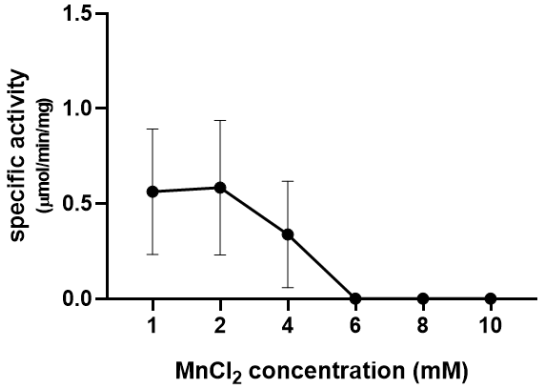

Figure 32: Specific initial activity of SufC based on concentration of $MnCl_2$. Graph shows an average of three independent measurements. error bars indicate standard deviation calculated by GraphPad Prism software.

5.5 Co-expression of SufB and SufC

SufB and SufC were co-expressed in pETDuet-1 expression vector, with an N-terminal 6x His-tag and a C-terminal 6x HA-tag, respectively. Co-expression was achieved by autoinduction in Rosetta2 *E. coli* cell line in a volume of 800 ml. The protein mixture was purified using Ni-NTA agarose and all fractions were analyzed using SDS-page and western blot (**Figure 33**). His-tagged SufB had an approximate molecular weight of 60 kDa and HA-tagged SufC had an approximate molecular weight of 40 kDa. Western blot with an anti-His-tag antibody (ThermoFisher) gave clear bands at the correct molecular weight, however western blot with an anti-HA-tag antibody (Roche) gives many clear bands of lower molecular weights.

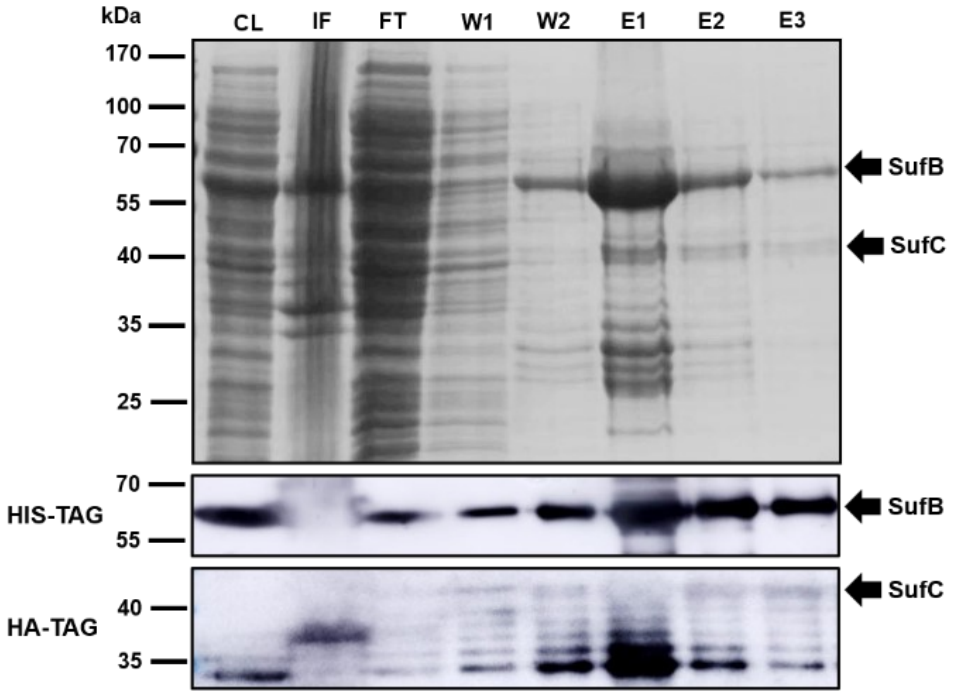

Figure 33: Purification fractions of SufB-SufC co-expression analyzed on Coommassie-stained SDS-PAGE gel (top image) and western blots of the purification gel stained by an anti-His tag antibody (middle image) and by an anti HA-tag antibody (bottom image). CL – cleared lysate, IF – insoluble fraction, FT – flow-through, W1, W2 – wash 1 and 2, E1, E2, E3 – elutions 1, 2 and 3.

5.5.1 Activity of SufC co-eluted with SufB

After the copurification of SufB with the SufC enzyme, the activity of SufC in the eluate was measured. This way I could make sure SufC is both present in the mixture in an intact active form and that purified SufC is active in the presence of SufB. **Figure 34** shows the progression curve of SufC activity in presence of SufB at pH 9.0, 50 mM NaCl and 8 mM $MgCl_2$. The specific ATPase activity (concentration of hydrolyzed ATP per min per mg of protein mixture) was 5.25 µmol/min/mg (an average of three independent measurements with a standard deviation 1.35).

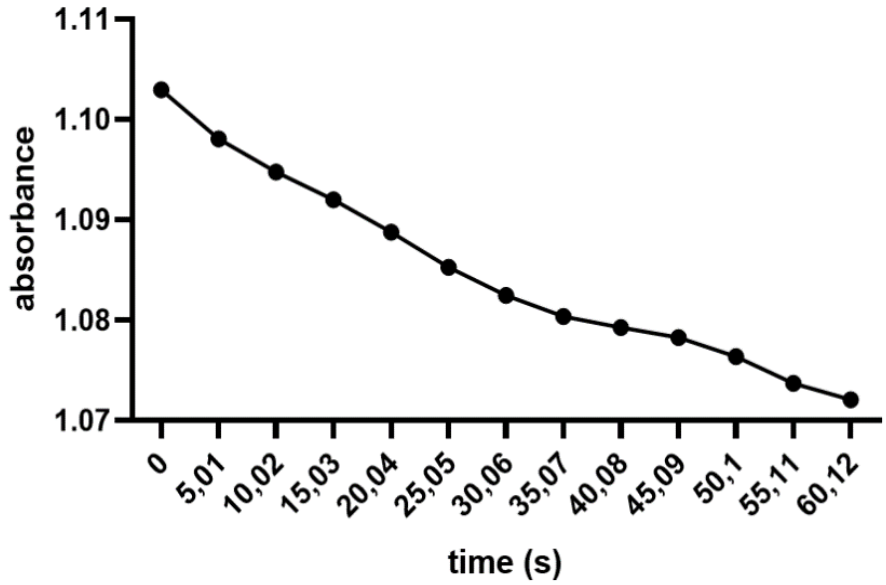

Figure 34: Progression curve of SufC activity in the presence with SufB. Graph shows the decrease of absorbance with time, which indicates ATPase activity.

5.5.2 Size exclusion chromatography

The mixture of SufB and SufC proteins isolated by affinity chromatography was separated according to size by size exclusion chromatography. Three runs using different elution buffers (300 mM NaCl, 1M NaCl and 300mM NaCl + 1mM ATP) were collected in 36 fractions. The resulting figures (**Figure 35-37**) show three chromatographs created by BioLogic DuoFlow software. Each peak represents UV absorption by a component of the protein mixture. Approximate molecular weights of each peak calculated from the calibration curve are listed in boxes above each peak. The numbers above the curve represent fraction numbers. Each fraction was analysed on SDS-PAGE gel. SDS-PAGE lanes below the chromatograph show the fractions corresponding to the fractions in the graph. All three runs confirmed the presence of a SufBC association.

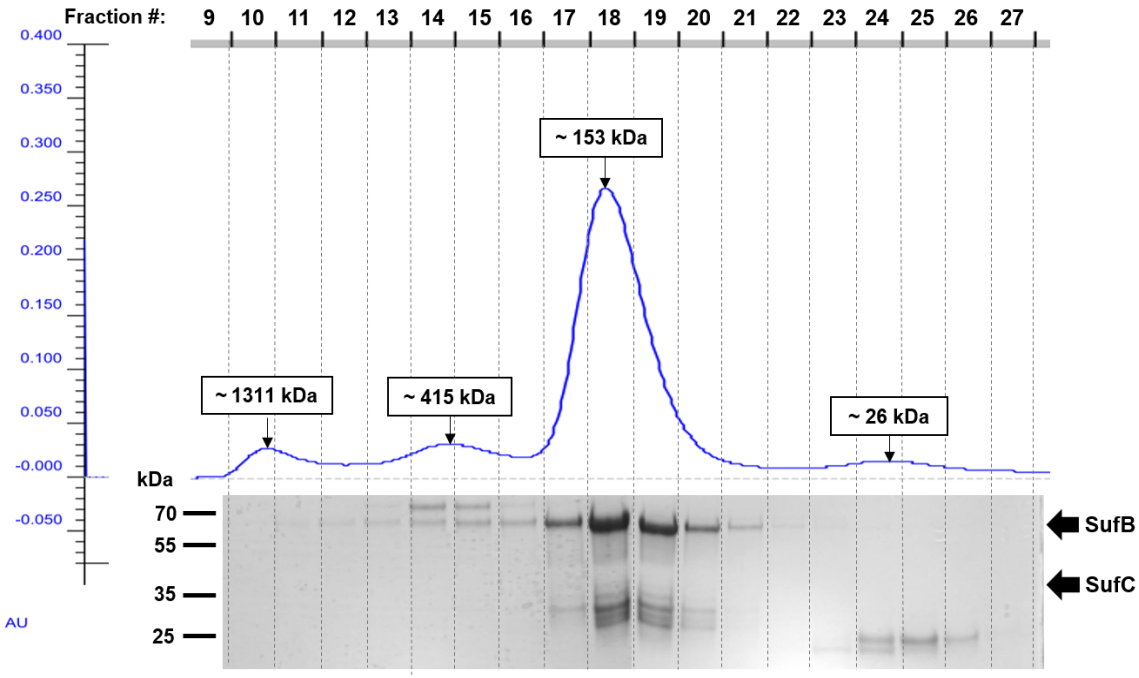

Figure 35: Size exclusion chromatography of purified *M. exilis* SufB and SufC, co-expressed in *E. coli* Rosetta2, in a buffer containing 300mM NaCl (50mM Hepes, pH 8.0, **300mM NaCl**, 10mM βME, 10% glycerol). Fraction number is indicated at the top X axis. Left axis (blue) denotes absorbance at 280 nm (blue curve). SDS-PAGE of corresponding fractions is shown below each fraction. SufB and SufC are indicated by arrows.

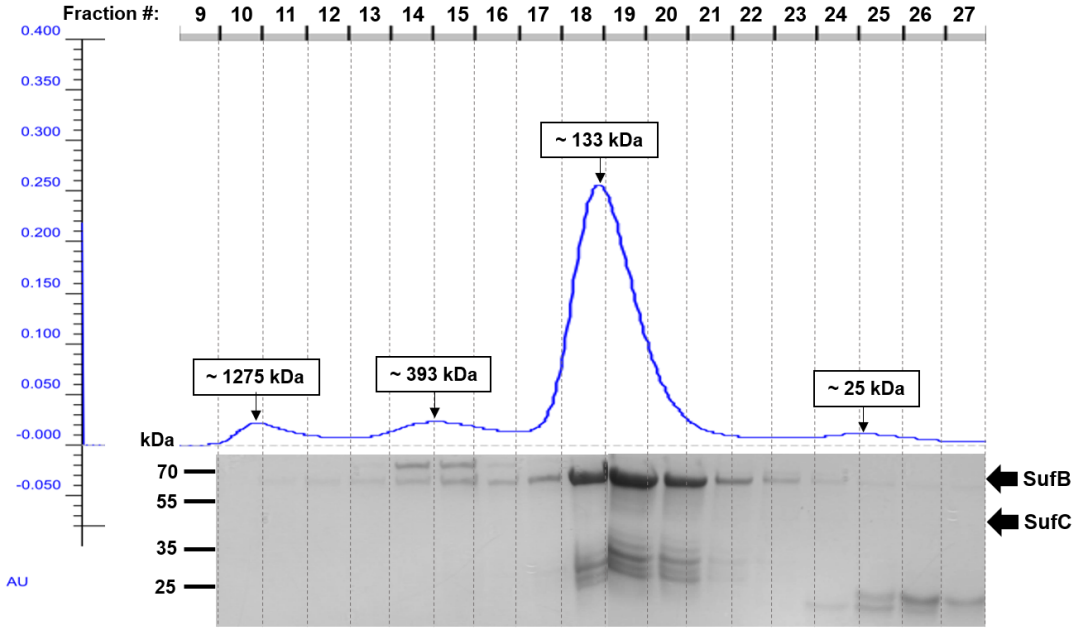

Figure 36: Size exclusion chromatography of purified *M. exilis* SufB and SufC, co-expressed in *E. coli* Rosetta2, in a buffer containing 1M NaCl (50mM Hepes, pH 8.0, **1M NaCl**, 10mM βME, 10% glycerol). Fraction number is indicated at the top X axis. Left axis (blue) denotes absorbance at 280 nm (blue curve). SDS-PAGE of corresponding fractions is shown below each fraction. SufB and SufC are indicated by arrows.

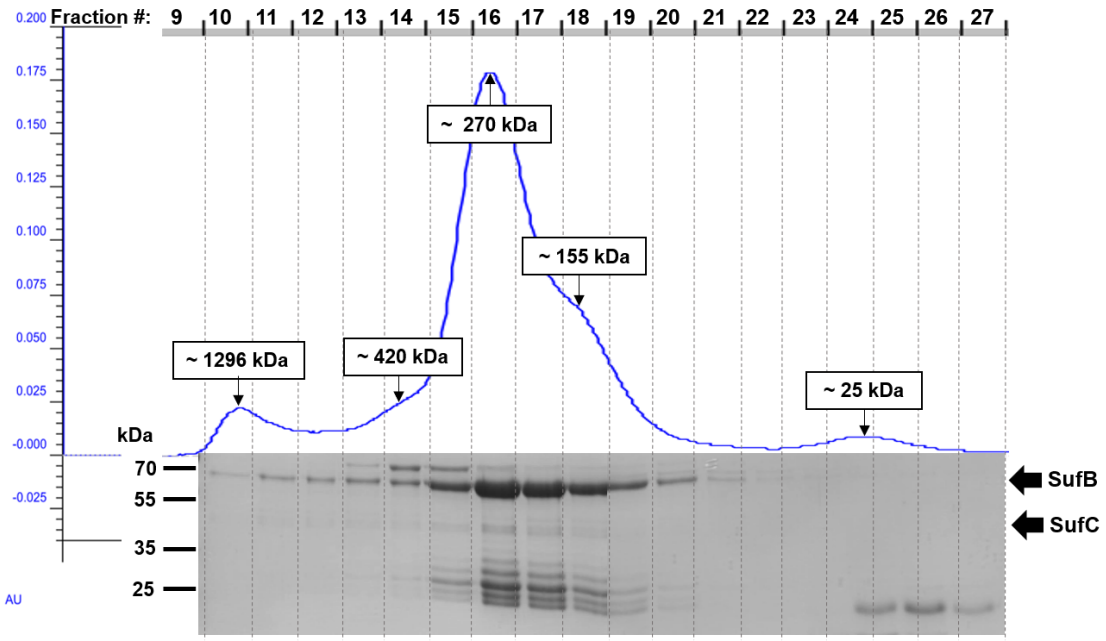

Figure 37: Size exclusion chromatography of purified *M. exilis* SufB and SufC, co-expressed in *E. coli* Rosetta2, in a buffer containing 300mM NaCl and 1mM ATP (50mM Hepes, pH 8.0, **300mM NaCl**, **1mM ATP** 10mM βME, 10% glycerol). Fraction number is indicated at the top X axis. Left axis (blue) denotes absorbance at 280nm (blue curve). SDS-PAGE of corresponding fractions is shown below each fraction. SufB and SufC are indicated by arrows.

6 Discussion

The SUF pathway has been the subject of numerous studies in bacteria, however, its presence in eukaryotic cells, apart from its presence in plastids, is a recent discovery. *M. exilis* and *P. pyriformis* are the first eukaryotic cells discovered to possess a complete SUF pathway instead of the canonical ISC. This finding together with the absence of mitochondria in *M. exilis* raised many questions. How does the pathway function in these cells? Does the fusion of SufD, SufS and SufU affect the complex formation? How does the SUF pathway communicate with the CIA pathway? And last but not least, where is the pathway localized in both of these organisms? Is the SUF pathway cytosolic in both *M. exilis* and *P. pyriformis*, even though one of these organisms possesses mitochondria and the other does not?

Addressing these questions is difficult using *Monocercomonoides,* as it is not a genetically tractable organism. Hence, an effort to answer these questions with *in vitro* assays was made by expressing SUF pathway proteins in recombinant form. Only after we are able to express and isolate the components of the pathway, we can use them to perform functional experiments. As a part of my thesis, I managed to optimize the conditions for heterologous expression of the recombinant version of two proteins from *M. exilis*, SufC and SufB. Both of these proteins were expressed in Rosetta2 *E. coli* cell line. The 6x His-tagged SufC was expressed using pET30a expression plasmid in E. coli Rosetta2, yielding large quantities of the protein in soluble form. Similarly, a 6x His-tagged SufB was co-expressed with 6x HA-tagged SufC in pETDuet-1 vector.

For the localization of the SUF pathway in *M. exilis* and *P. pyriformis,* a rabbit antibody against recombinant *M. exilis* SufC has been produced by our collaborators. When testing the antibody by western blot analysis on *P. pyriformis* and *M. exilis* cell lysates, the antibody detected a large band of approximately 100 kDa in *P. pyriformis* lysate. Since the expected size of SufC is approximately 30 kDa in both *M. exilis* and *P. pyriformis*, it is safe to assume this antibody does not bind to SufC in *P. pyriformis* and instead gives an unspecific signal. On the other hand, in *M. exilis* this antibody detected multiple bands of approximately 30 kDa, 40 kDa and 50 kDa. Since some of these bands are near the expected molecular size of SufC, the possibility that one of them may indeed be SufC could not be ruled out based on western blot only. The specificity of the antibody was therefore tested using immunoprecipitation. These results suggested that the band observed at approximately 40 kDa is in fact actin, with a fold change (compared to the

control) of 38, meanwhile SufC, though it is detected, is detected in a mere 8 fold-change in *M. exilis* lysate.

The SUF pathway localization was assessed by immunofluorescence using the same antibody against recombinant *M. exilis* SufC. Since these experiments were done before the immunoprecipitation data was obtained, I wanted to test the specificity of the antibody on *T. vaginalis* TvT1 cells. The slides were prepared with TvT1 culture transfected with HA-tagged *M. exilis* SufC. This culture was kindly provided by Mgr. Zuzana Vaitová, Ph.D. and was previously used to predict the localization of the SUF pathway in *M. exilis* by heterologous expression (Karnkowska et al. 2016). The cells were stained by the antibody against SufC as well as an anti HA-tag antibody. If the anti SufC antibody detected the HA-tagged SufC produced by *T. vaginalis* cell, the signal detected by this antibody would overlap with the signal detected by an anti HA-tag antibody. Even though the anti SufC antibody gave a signal throughout the cell in a pattern similar to the one reported in Karnkowska et al., where SufC was detected by anti HA-tag antibody only, no signal was detected by the anti HA-tag antibody. This was most probably due to the loss of expression by the transfected cells and unspecific binding of the anti SufC antibody. When detecting SufC in *M. exilis* and *P. pyriformis* cells, the slides were prepared with the same fixation as the *T. vaginalis* control. This fixation technique, however, proved insufficient for both *M. exilis* and *P. pyriformis*. All *M. exilis* cells observed under the microscope were disrupted and only the nucleus stained with DAPI and the flagella remained intact. *P. pyriformis* cells were disrupted or misshapen as well, although less severely than in the case of *M. exilis* and the cytosol remained detectable in most of the cells. In both *M. exilis* and *P. pyriformis*, the antibody gave off strong signal in the flagella, suggesting once again unspecific binding of the antibody. Since the results of immunoprecipitation settled that the antibody has the highest affinity towards actin, it is safe to assume that none of the immunofluorescence photos show any signal coming from SufC, but rather from actin which is an abundant protein in essentially all eukaryotic cells. Moreover, apart from being localized in the cytosol, conventional actin has been found to associate with the inner dynein arm complexes within flagella (Hirono et al. 2003), explaining why the most signal has been detected in *M. exilis* and *P. pyriformis* flagella. Given these results, the immunofluorescence experiment was not repeated using different fixation techniques to obtain intact cells, as better-quality slides would not provide any more information about the localization of the SUF pathway with an unspecific antibody.

A 6x His-tagged version of SufB was successfully co-expressed with a 6x HA-tagged SufC in pETDuet vector. Previous attempts of expressing SufB on its own, which have been performed by my colleague Priscila Peňa-Diaz, Ph.D., only ever yielded the protein in an insoluble form. SufB-SufC co-expression provided us with SufB recombinant protein in a soluble form, as proven by its presence on the cleared lysate after ultracentrifugation at 100,000g for 1 hour (Staudinger and Bandrés 2003). This result also suggests that the interaction of SufB and SufC may aid in the folding of SufB. Interestingly, most reports of SufB overexpression in bacteria involved its co-expression with other components of the *suf* operon, and subsequent separation from the mixture, yet rarely SufB alone (Layer et al. 2007; Hirabayashi et al. 2015; Yuda et al. 2017, Garcia et al. 2019). The western blot analysis of the purification fractions showed a large clear band corresponding to SufB detected by the anti His-tag antibody. The anti HA-tag antibody detected multiple bands of smaller molecular weight than the recombinant SufC, suggesting extensive degradation of this protein. However, when trying to measure the ATPase activity of the whole protein mixture, the mixture still displayed ATPase activity, proposing that some SufC has conserved its activity regardless of its binding to the scaffold protein.

Since the purification of recombinant SufC was successfully done in a native state, I tested whether the enzyme possesses ATPase activity, which was previously reported for this enzyme in bacteria (Nachin et al. 2003; Petrovic et al. 2008; Tian, He, and Liu 2014). The recombinant SufC possessed ATPase activity, with the optimal conditions for the activity being pH 9.0, 50mM NaCl, and 8mM $MgCl_2$. The specific activity measured was quite low, with 1.18 μmol of hydrolyzed ATP/min/mg. However, the specific activity of SufC on its own was also previously reported in similar orders, for example, Nachin et al. report 0.3 μmol of inorganic phosphate/min/mg. Standardization of pH demonstrated a clear peak of activity at pH 9.0, which is unusually high for a protein with predicted cytosolic localisation, since cytosolic pH of eukaryotic cells is generally maintained at pH 7.0–7.4 (Madshus 1988). For example, the cytosolic pH of *Giardia intestinalis* is maintained at pH 6.7–7.1 (Biagini et al. 2001). Moreover, the ideal pH for ATPase activity of SufC from bacteria has been reported as pH 7.5 (Nachin 2003; Petrovic et al. 2008; Tian, He, and Liu 2014). This observation further increases the need to precisely establish the localisation of this protein in the cell. For ionic strength buffer standardization, different concentrations of NaCl and KCl were tested. The enzyme maintained a very similar level of activity in all measured salt concentrations, with a slight peak at 50mM

NaCl. Finally, the activity was measured in the presence of various metal compounds to determine which cofactor was favoured by the ATPase and what concentration leads to the optimal ATPase activity. Four divalent metals were tested in various concentrations, namely $MgCl_2$, $MnCl_2$, $ZnSO_4$, and $CoCl_2$. SufC displayed no measurable activity in the presence of $CoCl_2$, suggesting that SufC is incapable of functioning with Co^{2+} as a cofactor. Similarly, in the presence of $ZnSO_4$, no activity was detected, and the enzyme precipitated from the solution after some time, which manifested itself by the reaction mixture becoming cloudy, resulting in an increase of absorbance. Some activity was measured in the presence of lower concentrations of $MnCl_2$, but concentrations higher than 4mM caused the enzyme to precipitate from the solution in a similar manner to $ZnSO_4$. Finally, when measured in the presence of $MgCl_2$, SufC displayed a steady activity, which increased with concentration up to 4mM $MgCl_2$. Above this concentration of the cation, the activity did not change significantly, peaking ever so slightly at 8mM $MgCl_2$. This result suggests that SufC is able to use Mg^{2+} ions as its cofactor, which is in agreement with magnesium ions found in its crystal structure (Watanabe, Kita, and Miki 2005). Mg^{2+} is favoured as a cofactor by many other ATPases, such as the F_1-ATPase (Frasch 2000) and the Na^+/K^+ ATPase (Pilotelle-Bunner et al. 2009). Moreover, Mg^{2+} ions have been proven essential for phosphoryl transfer during ATP synthesis and hydrolysis (Voet and Voet 2010).

The review of literature revealed, that SufC activity can be increased upon the interaction with SufB (Petrovic et al. 2008; Tian, He, and Liu 2014). Petrovic et al. documented a 180-fold increase in activity upon SufC-SufB interaction, whereas Tian, He and Liu reported a mere 2-fold increase. *M. exilis* SufC ATPase activity was also increased upon the interaction with SufB. Under aforementioned conditions (pH 9.0, 50 mM NaCl, 8 mM $MgCl_2$) the specific activity of SufC alone was 1.18 μmol/min/mg (per mg of purified SufC), whereas the specific activity of SufC co-expressed with SufB under the same conditions was 5.25 μmol/min/mg (per mg of purified mixture of SufC and SufB). The SufB:SufC ratio in the protein sample is unknown and therefore the precise increase in the specific activity of SufC cannot be determined, but from this data, it can be concluded that there is at least 4.5-fold increase in activity of SufC in SufBC complex compared to SufC alone.

To examine the complex formation between the co-expressed SufB and SufC, the protein mixture has been analysed using size exclusion chromatography. Firstly, the mixture was analysed in buffer containing 300mM NaCl, which was the same buffer used

for protein purification. In this condition, the chromatograph detected two small peaks of a large molecular size (fractions 10 and 14), corresponding to approximately 1311 kDa and 415 kDa at the top of the peak, respectively. When analysed by SDS-PAGE, no bands were detected in fraction 10 and two bands of approximately 60 kDa and 70 kDa were detected in fraction 14. This suggests that SufB may be capable of forming very large complexes with itself, yet its amount was so low it was barely detected on the gel, suggesting its concentration in the complete mixture is negligible. The second peak (fraction 14) could suggest an association of His-SufB (60 kDa) in a multimer with a larger protein, which is visible on the gel as a second band right above SufB at around 70 kDa. 70 kDa is a size which could very well correspond to a chaperone contaminant such as Hsp70 (DnaK) from *E. coli.* Chaperones are the most common contaminants of recombinant proteins produced in bacteria (Rohman and Harrison-Lavoie 2000; Morales, Parcerisa, and Ceccarelli 2019). The largest detected peak (containing the majority of the protein) was detected in fraction 18, which represents a molecular weight of approximately 153 kDa. Since both SufB and SufC were detected on the SDS-PAGE gel in this fraction it can be concluded that these two proteins form a complex *in vitro*. The SufB:SufC stoichiometry can be estimated from the size of the eluted complex. The approximate molecular weight of His-SufB is consistently around 60kDa, whereas SufC-HA should be around 40 kDa in theory. However, HA-tagged SufC exhibited extensive degradation when co-expressed with SufB, and the majority of the protein was detected at 30 kDa. With this in mind, a $SufB_2C$ stoichiometry fits the size of the complex ideally. The last peak detected by the FPLC (fraction 24) was around 26 kDa, which was either contamination or a residue of SufC. It may be speculated that the HA-tag on the C-terminus of the protein could be unstable and hence cleaved and lost in solution, soon after purification.

To test the stability of the eluted complex, a second measurement was done in a buffer containing 1M NaCl. An unstable or transient complex would likely be disrupted in high concentrations of salt, due to the high ionic strength that would disrupt salt bridges between proteins. Most importantly, a peak representing the SufB-SufC complex (fraction 18) was still observed, with SufC detected in the fraction on SDS-PAGE, suggesting a stable binding of SufB to SufC. This peak was detected slightly later in the elution, with the corresponding molecular weight of approximately 133 kDa. The 20 kDa difference might be contributed to SufC degradation or an artefact in the measurement.

However, given this shift in size, the possibility that our complex exists in a $SuBC_2$ stoichiometry as well should not be omitted.

The last measurement was performed in a buffer containing 300mM NaCl and 1mM ATP in order to detect changes in the organization of the complex upon ATP hydrolysis by SufC. In presence of 1mM ATP, two major peaks were detected, one in fraction 16 with the size of approximately 270 kDa, which displayed a "shoulder" most probably due to the presence of two, very closely eluted peaks, and a second smaller one in a similar size to the previously measured complexes (fraction 18, ~155 kDa). This result suggests that the SufB-SufC complex changes its conformation *in vitro* into a large complex upon the ATPase activity of SufC. SufC has been documented to dimerize within the $SufBC_2D$ complex upon ATPase activity (Hirabayashi et al. 2015). Therefore, it can be proposed that this complex is a dimerization of the $SufB_2C$ or $SufBC_2$ complex, especially since a putative $SufB_2C$ lacks a second SufC to form the interaction.

The scaffold exists predominantly as a $SufBC_2D$ complex in most of the bacterial systems where it has been assessed. An *in vitro* interaction between SufB and SufC as well as between SufC and SufD has been documented to yield a $SufB_2C_2$ and $SufC_2D_2$ complex, respectively (Chahal and Outten 2012; Wada et al. 2009). This is not surprising since SufB and SufD are structural homologues, which bind to each other and each of these proteins have been known to bind one SufC (Hirabayashi et al. 2015). So far, there has been experimental evidence of the existence of neither $SufBC_2$ nor $SufB_2C$ complexes, but since *M. exilis* and *P. pyriformis* SufD is a part of a SufDSU fusion gene, chances are that both of the SUF subcomplexes function in a different manner to the one we know from bacteria. Whether SufD from a SufDSU fusion is cleaved upon translation to join the scaffold and yield a $SufBC_2D$ complex, should remain the subject of future experiments. Further experimentation should be also performed to determine the stoichiometry of *M. exilis* SufB and SufC binding more accurately, and to rule out the existence of SufB and SufC in a $SufBC_2$ complex, as it is not certain which functional residues could take place in the binding of a second SufC to SufB. That being said, these data provide us valuable insight into the functionality of the SUF pathway in *M. exilis* and *P. pyriformis*.

7 Conclusion

This thesis was focused on the SUF pathway of *M. exilis* and *P. pyriformis.* To briefly summarize, these results were obtained:

1) A recombinant version of *M. exilis* SufC was prepared successfully in a native state.

2) Antibody production against *M. exilis* SufC was unfortunately not successful since the resulting antibody had a higher affinity towards actin than towards SufC. The localization of the SUF pathway in the cells of *M. exilis* and *P. pyriformis* is therefore still waiting to be settled.

3) The recombinant SufC showed ATPase activity and the conditions for the activity were standardized as pH 9.0, 50mM NaCl, and 8mM $MgCl_2$. The activity increased at least 4.5x upon the interaction with SufB.

4) SufB was successfully co-expressed with SufC. These two proteins formed a stable complex *in vitro.* Size exclusion chromatography analysis suggested a possible stoichiometry of the complex to be $SufBC_2$ or $SufB_2C$ which putatively dimerises in the presence of ATP.

8 Literature

Adinolfi, S., Iannuzzi, C., Prischi, F., Pastore, C., Iametti, S., Martin, S. R., Bonomi, F., and Pastore, A. (2009). Bacterial frataxin CyaY is the gatekeeper of iron-sulfur cluster formation catalyzed by IscS. *Nature Structural & Molecular Biology* **16**, 390–96.

Albrecht, A. G, Netz, D. J. A., Miethke, M., Pierik, A. J., Burghaus, O., Peuckert, F., Lill, R., and Marahiel, M. A. (2010). SufU is an essential iron-sulfur cluster scaffold protein in *Bacillus subtilis*. *Journal of Bacteriology* **192**, 1643–51.

Ali, V. and Nozaki, T. (2013). Iron-sulphur clusters, their biosynthesis, and biological functions in protozoan parasites. *Advances in Parasitology* **83**, 1–92.

Ali, V., Shigeta, Y., Tokumoto, U., Takahashi, Y., and Nozaki, T. (2004). An intestinal parasitic protist, *Entamoeba histolytica*, possesses a non-redundant nitrogen fixation-like system for iron-sulfur cluster assembly under anaerobic conditions. *Journal of Biological Chemistry* **279**, 16863–74.

Beinert, H., Holm, R. H., and Münck, E. (1997). Iron-sulfur clusters: nature's modular, multipurpose structures. *Science* **277**, 653–59.

Biagini, G. A., Knodler, L. A., Saliba, K. J., Kirk, K., and Edwards, M. R. (2001). Na^+-dependent pH regulation by the amitochondriate protozoan parasite *Giardia intestinalis*. *Journal of Biological Chemistry* **276**, 29157–62.

Black, K. A. and Dos Santos, P. C. (2015). Shared-intermediates in the biosynthesis of thio-cofactors: mechanism and functions of cysteine desulfurases and sulfur acceptors. *Biochimica et Biophysica Acta - Molecular Cell Research* **1853**, 1470–80.

Blanc, B., Clémancey, M., Latour, J. M., Fontecave, M., and Ollagnier De Choudens, S. (2014). Molecular investigation of iron-sulfur cluster assembly scaffolds under stress. *Biochemistry* **53**, 7867–69.

Boniecki, M. T., Freibert, S. A., Mühlenhoff, U., Lill, R., and Cygler, M. (2017). Structure and functional dynamics of the mitochondrial Fe/S cluster synthesis complex. *Nature Communications* **8**, 1287.

Brancaccio, D., Gallo, A., Mikolajczyk, M., Zovo, K., Palumaa, P., Novellino, E., Piccioli, M., Ciofi-Baffoni, S., and Banci, L. (2014). Formation of [4Fe-4S] clusters in the mitochondrial iron–sulfur cluster assembly machinery. *Journal of the American Chemical Society* **136**, 16240–50.

Braymer, J. J. and Lill, R. (2017). Iron–sulfur cluster biogenesis and trafficking in mitochondria. *Journal of Biological Chemistry* **292**, 12754–63.

Broderick, J B. (2003). "Iron–sulfur clusters in enzyme catalysis" in McCleverty, J. A. and Meyer, T. J. (ed.) *Comprehensive Coordination Chemistry 2nd edition*, Elsevier: Volume **8**, 739-757.

Carlton, J. M., Hirt, R. P., Silva, J. C., Delcher, A. L., Schatz, M., Zhao, Q., Wortman, J. R., Bidwell, S. L., Alsmark, U. C. M., Besteiro, S., Sicheritz-Ponten, T., Noel, C. J. et al. (2007). Draft genome sequence of the sexually transmitted pathogen *Trichomonas vaginalis*. *Science* **11**, 207–12.

Carlton, J. M., Hirt, R. P., Silva, J. C., Delcher, A. L., Schatz, M., Zhao, Q., Wortman, J. R., Bidwell, S. L., Alsmark, U. C. M., Besteiro, S., Sicheritz-Ponten, T., Noel, C. J. et al. (2007). Draft genome sequence of the sexually transmitted pathogen *Trichomonas vaginalis*. *Science* **11**, 207–12.

Chahal, H. K. and Outten, F. W. (2012). Separate FeS scaffold and carrier functions for $SufB_2C_2$ and SufA during in vitro maturation of [2Fe2S] Fdx. *Journal of Inorganic Biochemistry* **116**, 126–34.

Chandramouli, K., Unciuleac, M. C., Naik, S., Dean, D. R., Huynh, B. H., and Johnson, M. K. (2007). Formation and properties of [4Fe-4S] clusters on the IscU scaffold protein. *Biochemistry* **46**, 6804–11.

Cupp-Vickery, J. R., Urbina, H., and Vickery, L. E. (2003). Crystal structure of IscS, a cysteine desulfurase from *Escherichia coli*. *Journal of Molecular Biology* **330**, 1049–59.

Dawson, S. C., Pham, J. K., House, S. A., Slawson E. E., Cronembold, D., and Cande, Z. (2008). Stable transformation of an episomal protein-tagging shuttle vector in the piscine diplomonad *Spironucleus vortens*. *BMC Microbiology* **8**, 1471–2180.

Denoeud, F., Roussel, M., Noel, B., Wawrzyniak, I., Da Silva, C., Diogon, M., Viscogliosi, E., Brochier-Armanet, C., Couloux, A., Poulain, J., Segurens, B. et al. (2011). Genome sequence of the stramenopile *Blastocystis*, a human anaerobic parasite. *BMC Genome Biology* **12**, 1474–760.

Diamond, L S. (1957). The establishment of various trichomonads of animals and man in axenic cultures. *Journal of Parasitology* **43**, 488–490.

Diamond, L.S. (1982). A new liquid medium for xenic cultivation of *Entamoeba histolytica* and other lumen-dwelling protozoa. *The Journal of Parasitology* **68**, 958–959.

Doležal, P., Dagley, M. J., Kono, M., Wolynec, P., Likić, V. A., Foo, J. H., Sedinová, M., Tachezy, J., Bachmann, A., Bruchhaus, I., and Lithgow, T. (2010). The essentials of protein import in the degenerate mitochondrion of *Entamoeba histolytica*. *PLOS Pathogens* **6**, e1000812.

Dunkle, J. A., Bruno, M. R., Outten, F. W., and Frantom, P. A. (2019). Structural evidence for dimer-interface-driven regulation of the type II cysteine desulfurase, SufS. *Biochemistry* **58**, 687–96.

Frasch, W. D. (2000). The participation of metals in the mechanism of the F1-ATPase. *Biochimica et Biophysica Acta (BBA) - Bioenergetics* **1458**, 310–25.

Freibert, S. A., Goldberg, A. V., Hacker, C., Molik, S., Dean, P., Williams, T. A., Nakjang, S., Long, S., Sendra, K., Bill, E., Heinz, E., Hirt, R. P. et al. (2017). Evolutionary conservation and in vitro reconstitution of microsporidian iron-sulfur cluster biosynthesis. *Nature Communications* **8**, 1–12.

Fujishiro, T., Terahata T., Kunichika, K., Yokoyama, N., Maruyama, C., Asai, K., and Takahashi, Y. (2017). Zinc-ligand swapping mediated complex formation and sulfur transfer between SufS and SufU for iron–sulfur cluster biogenesis in *Bacillus subtilis*. *Journal of the American Chemical Society* **139**, 18464–67.

Garcia, P. S., Gribaldo, S., Py, B., and Barras, F. (2019). The SUF system: an ABC ATPase-dependent protein complex with a role in Fe-S cluster biogenesis. *Research in Microbiology* **170**, 426–34.

Goldberg, A. V., Molik, S., Tsaousis, A. D., Neumann, K., Kuhnke, G., Delbac, F, Vivares, C. P., Hirt, R. P., Lill, R., and Embley, T. M. (2008). Localization and functionality of microsporidian iron-sulphur cluster assembly proteins. *Nature* **452**, 624–28.

Gupta, V., Sendra, M., Naik, S. G., Chahal, H. K., Huynh, B. H., Outten, F. W., Fontecave, M., and Ollagnier de Choudens, S. (2009). Native *Escherichia coli* SufA, coexpressed with SufBCDSE, purifies as a [2Fe−2S] protein and acts as an Fe-S transporter to Fe-S target enzymes. *Journal of the American Chemical Society* **1311**, 6149–53.

Hamann, E., Gruber-Vodicka, H., Kleiner, M., Tegetmeyer, H. E., Riedel, D., Littmann, S., Chen, J., Milucka, J., Viehweger, B., Becker, K. W., Dong, X., Stairs, C. W. et al. (2016). Environmental Breviatea harbor mutualistic *Arcobacter* epibionts. *Nature* **534**, 254–58.

Hampl, V. (2017). "Preaxostyla." in Archibald, J. M., Simpson, A. G. B. and Slamovits, C. H. (ed.) *Handbook of the Protists,* Springer International Publishing, 1139–74.

Hirabayashi, K., Yuda, E., Tanaka, N., Katayama, S., Iwasaki, K., Matsumoto, T., Kurisu, G., Outten, F. W., Fukuyama, K., Takahashi, Y., and Wada, K. (2015). Functional dynamics revealed by the structure of the SufBCD complex, a novel ATP-binding cassette (ABC) protein that serves as a scaffold for iron-sulfur cluster biogenesis. *Journal of Biological Chemistry* **290**, 29717–31.

Hirono, M., Uryu, S., Ohara, A., Kato-Minoura, T., and Kamiya, R. (2003). Expression of conventional and unconventional actins in *Chlamydomonas reinhardtii* upon deflagellation and sexual adhesion. *Eukaryotic Cell* **2**, 486–93.

Hoff, K. G., Cupp-Vickery, J. R., and Vickery, L. E. (2003). Contributions of the LPPVK motif of the iron-sulfur template protein IscU to interactions with the Hsc66-Hsc20 chaperone system. *Journal of Biological Chemistry* **278**, 37582–89.

Hrdý, I., Hirt, R. P., Doležal, P., Bardonová, L., Foster, P. G., Tachezy, J., and Embley, T. M. (2004). *Trichomonas* hydrogenosomes contain the NADH dehydrogenase module of mitochondrial complex I. *Nature* **432**, 618–22.

Jacobson, M. R., Cash, V. L., Weiss, M. C., Laird, N. F., Newton, W. E., and Dean, D. R. (1989). Biochemical and genetic analysis of the NifUSVWZM cluster from *Azotobacter vinelandii*. *Molecular & General Genetics* **219**, 49–57.

Jedelský, P. L., Doležal, P., Rada, P., Pyrih, J., Šmíd, O., Hrdý, I., Šedinová, M. et al. (2011). The minimal proteome in the reduced mitochondrion of the parasitic protist Giardia intestinalis. *PLoS ONE* **6**, e17285.

Kaiser, J. T., Clausen, T., Bourenkow, G. P., Bartunik, H. D., Steinbacher, S., and Huber, R. (2000). Crystal structure of a NifS-like protein from *Thermotoga maritima*: implications for iron sulphur cluster assembly. *Journal of Molecular Biology* **297**, 451–64.

Karnkowska, A., Vacek, V., Zubáčová, Z., Treitli, S. C., Petrželková, R., Eme, L., Novák, L., Žárský, V., Barlow, L. D., Herman, E. K., Soukal, P., Hroudová, M. et al. (2016). A eukaryote without a mitochondrial organelle. *Current Biology* **26**, 1274–84.

Kelly, S., Reed, J., Kramer, S., Ellis, L., Webb, H., Sunter, J., Salje, J., Marinsek, N., Gull, K., Wickstead, B., and Carrington, M. (2007). Functional genomics in *Trypanosoma brucei*: A collection of vectors for the expression of tagged proteins from endogenous and ectopic gene loci. *Molecular and Biochemical Parasitology* **154**, 103–9.

Kispal, G., Csere, P., Prohl, C., and Lill, R. (1999). The mitochondrial proteins Atm1p and Nfs1p are essential for biogenesis of cytosolic Fe/S proteins. *The EMBO Journal* **18**, 3981–89.

Lange, H., Kaut, A., Kispal, G., and Lill, R. (2000). A mitochondrial ferredoxin is essential for biogenesis of cellular iron-sulfur proteins. *PNAS* **97**, 1050–55.

Layer, G., Gaddam, S. A., Ayala-Castro, C. N., Ollagnier-de Choudens, S., Lascoux, D., Fontecave, M., and Outten, F. W. (2007). SufE transfers sulfur from SufS to SufB for iron-sulfur cluster assembly. *Journal of Biological Chemistry* **282**, 13342–50.

Leger, M. M., Eme, L., Hug, L. A., and Roger, A. J. (2016). Novel hydrogenosomes in the microaerophilic Jakobid *Stygiella incarcerata*. *Molecular Biology and Evolution* **33**, 2318–36.

Lill, R., Dutkiewicz, R., Freibert, S. A., Heidenreich, T., Mascarenhas, J., Netz, D. J., Paul, V. D., Pierik, A. J., Richter, N., Stumpfig, M., Srinivasan, V., Stehling, O. et al. (2015). The role of mitochondria and the CIA machinery in the maturation of cytosolic and nuclear iron-sulfur proteins. *European Journal of Cell Biology* **94**, 280–91.

Liu, Y., Sieprawska-Lupa, M., Whitman, W. B., and White, R. H. (2010). Cysteine is not the sulfur source for iron-sulfur cluster and methionine biosynthesis in the methanogenic archaeon *Methanococcus maripaludis*. *Journal of Biological Chemistry* **285**, 31923–29.

Loiseau, L., Gerez, C., Bekker, M., Ollagnier-de Choudens, S., Py, B., Sanakis, Y., Teixeira de Mattos, Y., Fontecave, M., and Barras, F. (2007). ErpA, an iron sulfur (Fe-S) protein of the A-type essential for respiratory metabolism in *Escherichia coli. PNAS* **104**, 13626–31.

Loiseau, L., Ollagnier-de-Choudens, S., Nachin, L., Fontecave, M., and Barras, F. (2003). Biogenesis of Fe-S cluster by the bacterial Suf system: SufS and SufE form a new type of cysteine desulfurase. *Journal of Biological Chemistry* **278**, 38352–59.

Madshus, I. H. (1988). Regulation of intracellular pH in eukaryotic cells. *Biochemical Journal* **250**, 1–8.

Mi-ichi, F., Yousuf, M. A., Nakada-Tsukui, K., and Nozaki, T. (2009). Mitosomes in *Entamoeba histolytica* contain a sulfate activation pathway. *PNAS* **106**, 21731–36.

Morales, E. S., Parcerisa, I. L., and Ceccarelli, E. A. (2019). A novel method for removing contaminant Hsp70 molecular chaperones from recombinant proteins. *Protein Science* **28**, 800–807.

Muhlenhoff, U., Gerber, J., Richhardt, N., and Lill, R. (2003). Components involved in assembly and dislocation of iron-sulfur clusters on the scaffold protein Isu1p. *The EMBO Journal* **22**, 4815–25.

Nachin, L., Loiseau, L., Expert, D., and Barras, F. (2003). SufC: an unorthodox cytoplasmic ABC/ATPase required for [Fe-S] biogenesis under oxidative stress. *The EMBO Journal* **22**, 427–37.

Nie, D. (1950). Morphology and taxonomy of the intestinal protozoa of the guinea-pig, *Cavia porcella*. *Journal of Morphology* **86**, 381–493.

Nývltová, E., Šuťák, R., Harant, K., Šedinová, M., Hrdý, I., Pačes, J., Vlček, C., and Tachezy, J. (2013). NIF-type iron-sulfur cluster assembly system is duplicated and distributed in the mitochondria and cytosol of *Mastigamoeba balamuthi*. *PNAS* **110**, 7371–76.

O'Kelly, C. J., Farmer, M. A., and Nerad, T. A. (1999). Ultrastructure of *Trimastix pyriformis* (Klebs) Bernard et al.: Similarities of *Trimastix* Species with Retortamonad and Jakobid flagellates. *Protist* **150**, 149–62.

Outten, F. W., Wood, M. J., Muñoz, F. M., and Storz, G. (2003). The SufE protein and the SufBCD complex enhance SufS cysteine desulfurase activity as part of a sulfur transfer pathway for Fe-S cluster assembly in *Escherichia coli*. *Journal of Biological Chemistry* **278**, 45713–19.

Patzer, S. I. and Hantke, K. (1999). SufS Is a NifS-like protein, and SufD is necessary for stability of the [2Fe-2S] FhuF protein in *Escherichia coli*. *Journal of Bacteriology* **181**, 3307–9.

Petrovic, A., Davis, C. T., Rangachari, K., Clough, B., Wilson, R. J. M., and Eccleston, J. F. (2008). Hydrodynamic characterization of the SufBC and SufCD complexes and their interaction with fluorescent adenosine nucleotides. *Protein Science* **17**, 1264–74.

Pilotelle-Bunner, A., Cornelius, F., Sebban, P., Kuchel, P. W., and Clarke, R. J. (2009). Mechanism of Mg^{2+} binding in the Na^{+},K^{+}-ATPase. *Biophysical Journal* **96**, 3753–61.

Pondarré, C., Antiochos, B. B., Campagna, D. R., Clarke, S. L., Greer, E. L., Deck, K. M., McDonald, A., Han, A. P., Medlock, A., Kutok, J. L., Anderson, S. A., Eisenstein, R. S. et al. (2006). The mitochondrial ATP-binding cassette transporter Abcb7 is essential in mice and participates in cytosolic iron–sulfur cluster biogenesis. *Human Molecular Genetics* **15**, 953–64.

Pyrih, J., Pyrihová, E., Kolísko, M., Stojanovová, D., Basu, S, Harant, K., Haindrich, A. C., Doležal, P., Lukeš, J., Roger, A. J., and Tachezy, J. (2016). Minimal cytosolic iron-sulfur cluster assembly machinery of *Giardia intestinalis* is partially associated with mitosomes. *Molecular Microbiology* **102**, 701–14.

Reuß, D. R., Commichau, F. M., Gundlach, J., Zhu, B., and Stülke, J. (2016). The blueprint of a minimal cell: *MiniBacillus*. *Microbiology and Molecular Biology Reviews* **80**, 955–87.

Richards, T. A. and Van der Giezen, M. (2006). Evolution of the Isd11–IscS complex reveals a single α-proteobacterial endosymbiosis for all eukaryotes. *Molecular Biology and Evolution* **23**, 1341–44.

Roche, B., Laurent A., Ezraty, B., Mandin, P., Py B., and Barras, F. (2013). Reprint of: iron/sulfur proteins biogenesis in prokaryotes: formation, regulation and diversity. *Biochimica et Biophysica Acta - Bioenergetics* **1827**, 923–37.

Roger, A. J., Muñoz-Gómez, S. A., and Kamikawa, R. (2017). The origin and diversification of mitochondria. *Current Biology* **27**, R1177–92.

Rohman, M. and Harrison-Lavoie, K. J. 2000. Separation of copurifying GroEL from glutathione-s-transferase fusion proteins. *Protein Expression and Purification* **20**, 45–47.

Sagan, L. (1967). On the origin of mitosing cells. *Journal of Theoretical Biology* **14**, 255–74.

Schneider, R. E., Brown, M. T., Shiflett, A. M, Dyall, S. D., Hayes, R. D., Xie, Y., Loo, J. A., and Johnson, P. J. (2011). The *Trichomonas vaginalis* hydrogenosome proteome is highly reduced relative to mitochondria, yet complex compared with mitosomes. *International Journal for Parasitology* **41**, 1421–34.

Schwartz, C. J., Djaman, O., Imlay, J. A., and Kiley, P. J. (2000). The cysteine desulfurase, IscS, has a major role in in vivo Fe-S cluster formation in *Escherichia coli*. *PNAS* **97**, 9009–14.

Selbach, B. P., Chung, A. H., Scott, A. D., George, S. J., Cramer, S. P., and Dos Santos, P. C. (2014). Fe-S cluster biogenesis in gram-positive bacteria: SufU is a zinc-dependent sulfur transfer protein. *Biochemistry* **53**, 152–60.

Sheftel, A. D., Stehling, O., Pierik, A. J., Elsässer, H. P., Mühlenhoff, U., Webert, H., Hobler, A., Hannemann, F., Bernhardt, R., and Lill, R. (2010). Humans possess two mitochondrial ferredoxins, Fdx1 and Fdx2, with distinct roles in steroidogenesis, heme, and Fe/S cluster biosynthesis. *PNAS* **107**, 11775–80.

Shi, R., Proteau, A., Villarroya, M., Moukadiri, Zhang, L., Trempe, J. F., Matte, A., Armengod, M. E., and Cygler, M. (2010). Structural basis for Fe-S cluster assembly and tRNA thiolation mediated by IscS protein-protein interactions. *PLoS Biology* **8**, e1000354.

Sieber, K. B., Bromley, R. E., and Dunning Hotopp, J. C. (2017). Lateral gene transfer between prokaryotes and eukaryotes. *Experimental Cell Research* **358**, 421–26.

Silberg, J. J., Tapley, T. L., Hoff, K. G., and Vickery, L. E. (2004). Regulation of the HscA ATPase reaction cycle by the co-chaperone HscB and the iron-sulfur cluster assembly protein IscU. *The Journal of Biological Chemistry* **279**, 53924–31.

Stairs, C. W., Eme, L., Brown, M. W., Mutsaers, C., Susko, E., Dellaire, G., Soanes, D. M., Van Der Giezen, M., and Roger, A. J. (2014). A SUF Fe-S cluster biogenesis system in the mitochondrion-related organelles of the anaerobic protist *Pygsuia*. *Current Biology* **24**, 1176–86.

Staudinger, R. and Bandrés, J. C. (2003). "Solubilization of chemokine receptors from cell membranes." in Selinsky, B. S. (ed.) *Membrane Protein Protocols*, New Jersey: Humana Press: 228:103–10.

Stemmler, T. L., Lesuisse, E., Pain, D., and Dancis, A. (2010). Frataxin and mitochondrial FeS cluster biogenesis. *Journal of Biological Chemistry* **285**, 26737–43.

Stenzel, D. J. and Boreham, P. F. (1996). *Blastocystis hominis* revisited. *Clinical Microbiology Reviews* **9**, 563–84.

Studier, F. W. (2005). Protein production by auto-induction in high-density shaking cultures. *Protein Expression and Purification* **41**, 207-34.

Tachezy, J. and Šmíd, O. (2007). "Mitosomes in parasitic protists." in Tachezy, J. (ed.) *Hydrogenosomes and Mitosomes: Mitochondria of Anaerobic Eukaryotes*, Springer, 201–30.

Tian, T., He, H., and Liu, X. (2014). The SufBCD protein complex is the scaffold for iron–sulfur cluster assembly in *Thermus thermophiles* HB8. *Biochemical and Biophysical Research Communications* **443**, 376–81.

Treitli, S. C., Kolisko, M., Husník, F., Keeling, P. J., and Hampl, V. (2019). Revealing the metabolic capacity of *Streblomastix strix* and its bacterial symbionts using single-cell metagenomics. *PNAS* **116**, 19675–84.

Treitli, S. C., Kotyk, M., Yubuki, N., Jirounková, E., Vlasáková, J., Smejkalová, P., Šípek, P., Čepička, I., and Hampl, V. (2018). Molecular and morphological diversity of the oxymonad genera *Monocercomonoides* and *Blattamonas* gen. nov. *Protist* **169**, 744–83.

Tsaousis, A. D., Ollagnier de Choudens, S., Gentekaki, E., Long, S., Gaston, D., Stechmann, A., Vinella, D., Py, B., Fontecave, S., Barras, F., Lukeš, J., and Roger, A. J. (2012). Evolution of Fe/S cluster biogenesis in the anaerobic parasite *Blastocystis*. *PNAS* **109**, 10426–31.

Urbina, H. D., Silberg, J. J., Hoff, K. G., and Vickery, L. E. (2001). Transfer of sulfur from IscS to IscU during Fe/S cluster assembly. *The Journal of Biological Chemistry* **276**, 44521–26.

Uzarska, M. A., Dutkiewicz, R., Freibert, S. A., Lill, R., and Mühlenhoff, U. (2013). The mitochondrial Hsp70 chaperone Ssq1 facilitates Fe/S cluster transfer from Isu1 to Grx5 by complex formation. *Molecular Biology of the Cell* **24**, 1830–41.

Vacek, V., Novák, L. V. F., Treitli, S. C., Táborský, P., Čepička, I., Kolísko, M., Keeling, P. J., and Hampl, V. (2018). Fe–S cluster assembly in Oxymonads and related protists. *Molecular Biology and Evolution* **35**, 2712–18.

Vinella, D., Brochier-Armanet, C., Loiseau, L., Talla, E., and Barras, F. (2009). Iron-sulfur (Fe/S) protein biogenesis: phylogenomic and genetic studies of A-type carriers. *PLoS Genetics* **5**, e1000497.

Voet, D. and Voet, J. G. (2010). *Biochemistry*. John Wiley & Sons.

Wada, K., Hasegawa Y., Gong, Z., Minami, Y., Fukuyama, K., and Takahashi, Y. (2005). Crystal structure of *Escherichia coli* SufA involved in biosynthesis of iron-sulfur clusters: implications for a functional dimer. *FEBS Letters* **579**, 6543–48.

Wada, K., Sumi, N., Nagai, R., Iwasaki, K., Sato, T., Suzuki, K., Hasegawa, Y., Kitaoka, S., Minami, Y., Outten, F. W., Takahashi, Y., and Fukuyama, K. (2009). Molecular dynamism of Fe–S cluster biosynthesis implicated by the structure of the SufC2–SufD2 complex. *Journal of Molecular Biology* **387**, 245–58.

Watanabe, S., Kita, A., and Miki, K. (2005). Crystal structure of atypical cytoplasmic ABC-ATPase SufC from *Thermus thermophilus* HB8. *Journal of Molecular Biology* **353**, 1043–54.

Wollers, S., Layer, G., Garcia-Serres, R., Signor, L., Clemancey, M., Latour, J. M., Fontecave, M., and Ollagnier De Choudens, S. (2010). Iron-sulfur (Fe-S) cluster assembly: the SufBCD complex is a new type of Fe-S scaffold with a flavin redox cofactor. *Journal of Biological Chemistry* **285**, 23331–41.

Xu, X. M. and Møller, S. G. (2011). Iron–sulfur clusters: biogenesis, molecular mechanisms, and their functional significance. *Antioxidants & Redox Signaling* **15**, 271–307.

Yuda, E., Tanaka, N., Fujishiro, T., Yokoyama, N., Hirabayashi, K., Fukuyama, K., Wada, K., and Takahashi, Y. (2017) Mapping the key residues of SufB and SufD essential for biosynthesis of iron-sulfur clusters. *Scientific Reports* **7**, 9387.